Catalysis Today 144 (2009) 219–234

Contents lists available at ScienceDirect

Catalysis Today

journal homepage: www.elsevier.com/locate/cattod

From single crystals to supported nanoparticles in experimental and theoretical studies of H_2 oxidation over platinum metals (Pt, Pd): Intermediates, surface waves and spillover

V.V. Gorodetskii *, A.A. Sametova, A.V. Matveev, V.M. Tapilin

Boreskov Institute of Catalysis, Pr. Ak. Lavrentieva 5, Novosibirsk 630090, Russia

ARTICLE INFO

Article history:
Available online 31 January 2009

Keywords:
H_2 oxidation
Intermediates
Pt(1 1 1)
Pt(1 0 0)
Pd(1 1 0)
Tips
Chemical wave
Nanoparticles
Hydrogen spillover
Field electron microscopy
Field ion microscopy
Density functional theory

ABSTRACT

The present paper reviews our investigations concerning the mechanism of $H_2 + O_2$ reaction on the metal surfaces (Pt, Pd) at different structures: single crystals (Pt(1 1 1), Pt(1 0 0), Pd(1 1 0)); microcrystals (Pt tips); and nanoparticles (Pd–Ti^{3+}/TiO_2). Field electron microscopy (FEM), field ion microscopy (FIM), high-resolution electron energy loss spectroscopy (HREELS), XPS, UPS, work function (WF), TDS and temperature-programmed reaction (TPR) methods have been applied to study the kinetics of H_2 oxidation on a nanolevel. The adsorption of both O_2 and H_2 and several dissociative products (H_{ads}, O_{ads}, OH_{ads}) was studied by HREELS. Using the DFT technique the equilibrium states and stretching vibrations of H, O, OH, H_2O, adsorbed on the Pt(1 1 1) surface, have been calculated depending on the surrounding of the metal atoms. Sharp tips of Pt, several hundreds angstroms in radius, were used to perform *in situ* investigations of the dynamic surface processes. The FEM and FIM studies on the Pt-tip surface demonstrate that the self-oscillations and waves propagations are connected with periodic changes in the surface structure of nanoplane (1 0 0)-(hex) ↔ (1 × 1), varying the catalytic property of metal. The role of defects (Ti^{3+}-$\square_O$) in the adsorption centers formation, their stabilization by the palladium nanoparticles, and then the defects participation in $H_2 + O_2$ steady-state reaction over Pd–Ti^{3+}/TiO_2 surface have been studied by XPS, UPS and photodesorption techniques (PhDS). This reaction seems to involve the "protonate" hydrogen atoms (H^+/TiO_x) as a result of spillover effect: diffusion of H_{ads} atoms from Pd particles on a TiO_x surface. The comprehensive study of H_2, O_2 adsorption and $H_2 + O_2$ reaction in a row: single crystals → tips → nanoparticles has shown the same nature of active centers over these metal surfaces.

1. Introduction

In the late 1950s Boreskov [1] stated a chemical approach to the kinetics of heterogeneous catalysis by metals based on the influence of the reaction mixture and reaction conditions on the properties and chemical composition of the catalyst. For a long time H_2 oxidation on the platinum group metals has been considered as a catalytic model reaction that can produce valuable information on the mechanism of such effects [2]. It is known that the most active metals in the oxidation of hydrogen are platinum and palladium catalysts [1–3]. As a consequence of the practical importance of this reaction, for example, fuel cells have up-to-date interest; numerous studies on platinum group metals can be found in literature. However, it has not been well established whether the water molecules formation corresponds to Langmuir–Hinshelwood (LH) mechanism, including H_2, O_2 dissociative adsorption with the formation of hydroxyl groups and subsequent reaction $H_{ads} + OH_{ads} \rightarrow H_2O_{ads}$ or hydroxyl disproportionation in the reaction $2OH_{ads} \rightarrow H_2O_{gas} + O_{ads}$ [4–10]. The kinetics of the reaction and the nature of the reaction intermediates on the Pt(1 1 1), Pd(1 1 1), Rh(1 1 1) and Rh(1 0 0) single crystal surfaces have been studied with the techniques of HREELS [9–14], scanning tunneling microscopy (STM) [15], TPR [8,10] and molecular beam (MB) [7,16,17]. The result of these investigations indicates that the hydrogen and oxygen are dissociatively chemisorbed on Pt, Pd and Rh surfaces. At low temperatures ($T < 200$ K) H_2O formation proceeds through sequential addition of hydrogen to oxygen with a hydroxyl intermediate. Direct evidence for adsorbed OH-groups on Pt(1 1 1) was given by HREELS [9,11,12,14]. The STM results [14,15] demonstrated that low temperature H_2 oxidation on the same platinum surface includes an autocatalytic process, leading to the formation of travel reaction fronts at oxygen island perimeters. The spectroscopic data [8–14,18] reveal that two pathways for water

* Corresponding author. Fax: +7 3832 308056.
E-mail address: matveev@catalysis.ru (V.V. Gorodetskii).

0920-5861/$ – see front matter © 2009 Elsevier B.V. All rights reserved.
doi:10.1016/j.cattod.2008.12.014

formation via rapid reaction of adsorbed hydrogen with the adsorbed hydroxyl, $H_{ads} + OH_{ads} \rightarrow H_2O_{ads}$, or via hydroxyl disproportionation, $2OH_{ads} \rightarrow H_2O_{gas} + O_{ads}$, could be considered. According to [14] the hydroxyl disproportionation may become important at low temperatures and high oxygen coverages, leading to an autocatalytic process. As was shown in ref. [17–20], the mechanism of H_2 oxidation (L–H) can consist of the following elementary steps:

(1) $H_{2\ gas} + 2^* \leftrightarrow 2H_{ads}$
(2) $O_{2\ gas} + 2^* \rightarrow 2O_{ads}$
(3) $O_{ads} + H_{ads} \rightarrow OH_{ads} + ^*$
(4) $H_{ads} + OH_{ads} \rightarrow H_2O_{ads} + ^*$
(5) $2OH_{ads} \rightarrow O_{ads} + H_2O_{ads}$
(6) $H_2O_{ads} \rightarrow H_2O_{gas} + ^*$

Theoretical calculations predicted the existence of bistability regions for H_2 oxidation reaction [21]. During hydrogen oxidation the formation of target patterns and the propagation of reaction-diffusion fronts were observed by spatially resolved (~1 μm) photoemission electron microscopy (PEEM). Chemical wave patterns at H_2 oxidation have been found on the Pt(1 0 0) [22], Rh(5 3 3) [23], Rh(1 1 1) [24], Rh(1 1 0)/Pt [25] surfaces by PEEM; on the Pt, Ir and Rh tip surfaces by FEM with the higher lateral resolution of ca. 20 Å [26–28] and FIM with near-atomic resolution of ca. 3/6 Å [29]; on the Pt(1 1 1) surface by STM [15]. Sharp tips (FEM/FIM) in size up to several hundreds of Angstroms have been used to investigate *in situ* the real dynamic surface processes where different crystallographic nanoplanes of the tip are simultaneously exposed to the reacting gas and for which it is possible to study the interaction and the coupling of adjacent planes [22]. FEM observations of the emitter tips in $H_2 + O_{ads}$ reaction demonstrate that the stepped nanoplanes (Pt(3 3 1), Ir(3 2 1), Rh(4 1 0)) are the most catalytically active regions and can act as nucleating centers for the initiation of the reaction fronts on adjacent planes [26–28]. Different regimes of catalytic activity and kinetic oscillations at certain control parameters (T, P_i) have been observed by FIM on the Pt and Rh tip surfaces [31–34]. In these studies the reacting gases (O_2, H_2) and product (H_2O) have been used to image the catalyst active centers *in situ*. The existence of a mobile reaction front between hydrogen and oxygen layers has been observed.

It is known that real metal/support catalysts usually consist of nano-sized metal particles on which different crystal planes are exposed. Therefore, the reaction kinetics on a supported metal catalyst might be quite different as compared to that on the single crystal surfaces, as a result of interplay between different nanoplanes present on small particles. These surfaces, with a particle size of 100–300 Å, are mainly formed by the densest (1 1 1), (1 0 0), (1 1 0) planes, which differ drastically towards the adsorption and oscillatory behavior. Pronounced crystallographic anisotropy observed in FEM experiments on the apex of the Pt-tip surface (exposing a wide variety of arrangements of active centers) makes the results highly relevant to real catalysts, including supported metals. It likely seems that the oxidation of hydrogen is an ideal reaction for the study of "spillover" hydrogen effects on the catalytic properties of supported metal catalysts. The metal modifying effect on the active centers properties in the supported metal catalysts is known to be realized by: (i) strong metal support interaction (SMSI) [35]; (ii) dimensional change of particles size [36]; (iii) defects formation on a support surface [37]; (iv) metal → support hydrogen "spillover" phenomena [38]. Two main mechanisms – for instance an electron transfer from Ti^{3+} to Pt [39] and encapsulation of the metal particles by supported titanium oxide species [40] – have been proposed to explain the modifying effect of catalytic properties induced by SMSI. As a rule, the stoichiometric oxide surface (TiO_2) is supposed to be catalytically inactive, whereas the supported metals (Pt, Pd) present a highly active part of the catalytic system. Reduction of the TiO_2 surface leads to the formation of the Ti^{3+}-$\square_O$ type defects ($\square_O$ is an oxygen-vacancy), which are responsible for the molecularly adsorbed O_2 species [41,42]. "Spillover" process involves a diffusion of hydrogen atoms, generated via dissociative chemisorption of molecular hydrogen on the metal particles (Pt, Pd), into the support of this bifunctional catalyst. In the "spillover" regime, the reaction mixture affects the properties of the support defect surfaces. Clearly, the overall kinetics of H_2 oxidation is quite complex and still not fully understood, in particular because the participation of "spillover" H_{ads} atoms, produced by H_2 dissociation on metal, on the TiO_x surface needs to be considered for this reaction [43].

In the present contribution we report the results of our studies of the mechanism of H_2 oxidation on various levels of catalytic systems beginning from the molecular level (intermediates) and to bridge the *structure* (or materials) gap [44] between the single crystal (Pt(1 1 1), Pt(1 0 0), Pd(1 1 0)), sharp tip (Pt, Pd) and nano-size supported metal particle (Pd–Ti^{3+}/TiO_2) surfaces under the low-pressure reaction conditions. FEM, FIM, HREELS, XPS, UPS and TPR have been applied to the study of the kinetics of H_2 oxidation. The adsorption of both O_2 and H_2 and several dissociative products (H_{ads}, O_{ads} and OH_{ads}) was studied by HREELS and WF. Using the techniques of density functional theory (DFT) the equilibrium states and stretching vibrations of H_{ads}, O_{ads} atoms and OH_{ads}, H_2O_{ads} molecules, adsorbed on the Pt(1 1 1), have been calculated depending on the surrounding of the metal atoms. Sharp tips of Pd and Pt were used to perform *in situ* investigations of dynamic surface processes. The role of defects (Ti^{3+}-$\square_O$) in the active centers formation, their stabilization by the palladium nanoparticles, and then defects participation in $H_2 + O_2$ reaction over Pd–Ti^{3+}/TiO_2 surface ("spillover" effect) were studied by XPS, UPS and photodesorption techniques. The comprehensive study of H_2, O_2 adsorption and $H_2 + O_{ads}$ titration reaction on single crystals (Pt(1 1 1), Pt(1 0 0), Pd(1 1 0)), microcrystals (Pt, Pd tips), nanoparticles (Pd–Ti^{3+}/TiO_2) will allow an understanding of the nature of active centers over these metal surfaces. The direct comparison of catalytic properties of nanosized planes (supported Pd particles, ca. 20 Å), with those of sharp tips (ca. 10^3 Å) and extended single crystal surfaces (ca. 10^8 Å) gives the possibility to bridge the "*structure gap*" between single crystal surfaces and metal nanoparticles, and to establish the intrinsic interrelation of reaction mechanism of the hydrogen oxidation on these surfaces.

2. Experimental techniques

2.1. Experimental techniques in HREELS and TPR

The HREELS, XPS, UPS, TDS, TPR, FIM and FEM experiments were performed in three separate ultrahigh vacuum (UHV) chambers with a base pressure below 10^{-10} mbar. The energy loss spectra were obtained at the specular direction by using a VG ADES 400 electron spectrometer, an electron energy of ca. 2.5 eV and an incident angle of ca. 35° with respect to the surface normal. The resolution of the elastically reflected beam was about 9–11 meV (ca. 70–90 cm^{-1}). The TPR spectra were measured with a quadrupole mass spectrometer (QMS) by using a heating rate of 6–10 K s^{-1}. The cleaning procedure of the Pt(1 1 1), Pt(1 0 0) and Pd(1 1 0) surfaces included Ar^+ etching and annealing cycles in oxygen and in vacuum. The crystal was exposed to H_2 or O_2 molecular beam by using a capillary array dozer. The gas flow was controlled by quadrupole mass spectrometry and calibrated by comparison of the areas under flash desorption curves obtained by adsorbing H_2 using the beam set-up and the conditions under

equilibrium hydrogen pressure. The structure of the clean single crystal surfaces was confirmed by LEED. The temperature of the single crystals was measured by means of chromel/alumel thermocouples spotwelded to the sample, and could be controlled to within 1 K by using a heating power supply with a feedback loop. The reaction gases, H_2 and O_2, were of the highest purity available, and were always checked by a mass spectrometry before use. The experimental setup has been described in detail elsewhere [45–47].

2.2. Experimental techniques in FEM and FIM

Field electron and field ion microscope experiments were performed in a second UHV system, which was used simultaneously as a flow catalytic reactor. Details of the Pt-tip preparation of sharp radius (ca. 10^3 Å) have been given elsewhere [48] (Fig. 1a). Depending on tip-radius preparation, different crystallographic nanoplanes may have a linear dimension from 50 to 200 Å. The Pt surface was cleaned by field evaporation and characterized with the field electron microscope at a field of ca. 0.3 V/Å, tip radius r = 680 Å, applied voltage at $V \sim 1$ kV (Fig. 1b). Another procedure for cleaning Pt tips consists in several cycles of thermal annealing to 1000 K at 10^{-10} mbar and subsequent Xe-ion sputtering in the FEM regime in the presence of $P_{Xe} \approx 10^{-3}$ mbar [49]. In the FEM experiments, a negative voltage V is applied to a metal tip. Upon increasing the field strength, both the height and the width of the energy barrier decrease. Electrons are emitted into vacuum from the tip by tunneling through a potential barrier at the surface by the applied field and are accelerated towards a fluorescent screen. A single or double channel plates were used as an image amplifier of a small electron emission current (<1 nA), and a CCD camera with a time resolution of 40 ms recorded *in situ* the dynamic behavior of surface processes [48,49]. The field electron current (FEM) measures local properties of a surface with a lateral resolution of ca. 20 Å and magnification of ca. 3×10^5. The *in situ* measurement of surface reactivity, which is combined with work function alterations, concerns different surface orientations simultaneously. Electrostatic field effects at the ca. 0.3 V/Å level used during these investigations are low enough not to affect the studied surface chemistry [50]. In terms of the FEM experiments, the surface analysis of the field tip emitter is based on the changes in local work function ($\Delta\varphi$) accompanying adsorption of H_2 and oxygen, which can be correlated with the total field electron currents, as described before [51]. The surface planes of Pt show an increase of $\Delta\varphi$ with the adsorption of hydrogen ($\Delta\varphi \approx 0.2$ eV) and an even higher increase after the adsorption of oxygen ($\Delta\varphi \approx 1.2$ eV) [26,48]. This large change in $\Delta\varphi$ gives an excellent tool for distinguishing transition in the adsorption layers: the oxygen adsorption layer with low emission current and hydrogen adlayer with high emission current. The brightness of local regions of FEM images is connected with the most reactive surface areas. The FEM experimental device, based on the use of sharp field emitter tips, was described before [51,52].

Mainly noble gases (He, Ne) have been used in the field ion microscope to produce atomically resolved surface sites of the field emitter tip [53]. The high electric field strength is required for imaging of Pt-tip surface in Ne ions. When the applied field at the tip approaches $F \sim 3.5$ V/Å for ionization of Ne, neon atoms at the surface may lose a valence electron to the metal by tunneling. The positive ions (Ne^+) accelerate from the tip surface in a radial direction to the screen. A high lateral resolution of ca. 3 Å is achieved at low temperature (78 K) by Ne^+ imaging (Fig. 1c). In our studies, instead of applying usual imaging gases (He, Ne) the reaction gas mixture itself is used to image the surface [22,34]. As it will be shown later, the unexpected surface specificity in the gas mixture imaging results in a new informative method displaying directly catalytically reacting surfaces *in situ* at near-atomic resolution. Chemical analysis of the surface processes involved in $H_2 + O_2$ and $CO + O_2$ oscillating reactions has been obtained by applying field- and laser-pulse desorption mass-spectrometry [54,55] or by analyzing the field ion current with mass spectrometric techniques [52]. In the first case, a surface analysis of adsorption layers is possible [55]. In the second case, ionized desorption products of the catalytic reaction are analyzed by mass spectrometry [52]. The electrostatic field strength for imaging the surface in these reactions by FIM was in interval from $F \approx 1.0$ V/Å to 1.5 V/Å.

The field emission and field ionization microscopes were operated with low electron and ion currents (ca. 0.1 nA) to minimize collisions of gas molecules. The temperature at the tip could be controlled to within 1 K and was measured by means of a chromel/alumel thermocouple spot-welded to the metal loop near the tip. The reaction gases H_2 and O_2 of the highest purity were introduced and measured with a quadrupole mass spectrometer. The FEM image and total field electron current were continuously monitored during the catalytic surface reaction at an oxygen partial pressure of ca. 10^{-4} mbar and hydrogen partial pressure of ca. 10^{-4} mbar. It was demonstrated that at a pressure of up to ca. 10^{-4} mbar, stable emission currents could be obtained and the sputtering processes seem to be completely negligible.

2.3. Experimental techniques in XPS, UPS and photodesorption studies

The UPS (He I) and XPS (Mg Kα) measurements were carried out in a third UHV chamber that is equipped with a VG ESCA-3

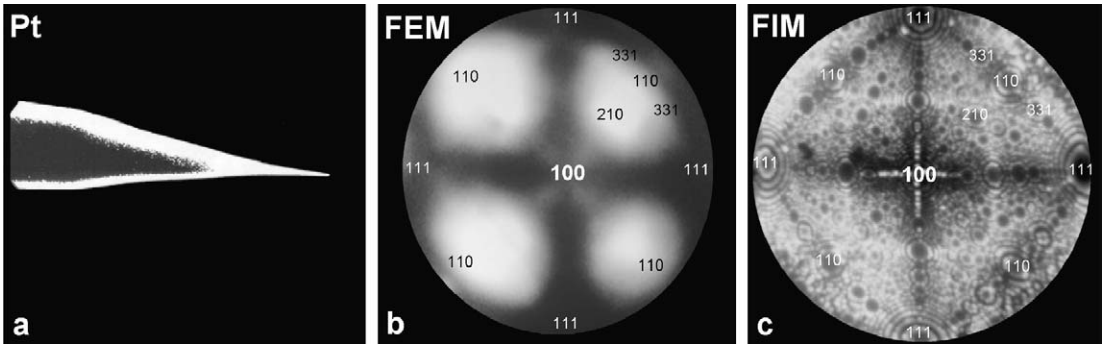

Fig. 1. (a) Transmission electron image of Pt-tip used for investigations of the oscillating H_2 oxidation. Field electrons in the FEM or field ions in the FIM from the tip are impinging at the detector consisting of a high sensitivity channel plate and a screen. The images are recorded with a video camera. (b) FEM-image [100]-oriented Pt-tip, ~1 kV, $F \sim 0.3$ V/Å. (c) FIM image of the same Pt-tip imaged with Ne^+ at 78 K; field evaporated at 16.5 kV; best image voltage at 15 kV, $P_{Ne} = 2 \times 10^{-4}$ mbar; tip radius, r = 680 Å, $F \sim 3.5$ V/Å [29].

photoelectron spectrometer and QMS. The Pd–Ti^{3+}-$\square_O/TiO_2$ model system was prepared by a successive vacuum evaporation of palladium onto a flat thin oxide layer (Ti^{3+}/TiO_2) formed on the clean titanium foil (Ar^+ etching) upon oxygen adsorption of 10^3 ML (T = 900 K, $P(O_2) = 10^{-2}$ mbar), and reduction by heating in vacuum at $T \sim 700$ K [43]. The photoelectron spectrum of the surface shows titanium, oxygen and palladium lines only. According to XPS (Pd $3d_{5/2}$) and TDS ($H_{ads}/Pd/TiO_x$) data the θ_{Pd} value is 0.3 ML (1 ML = 1×10^{15} atoms cm^{-2}).

The catalytic activity of Pd/TiO_x system at H_2 oxidation was studied in a separate all-glass ultrahigh vacuum apparatus (1.5 L volume). Reaction gases such as H_2 and O_2 of the highest purity were introduced with a flow rate of ca. 1.5 L s^{-1}, and controlled by the mass spectrometer. The rate measurements of the $H_2 + O_2$ reaction were described in ref. [56]. The Ti foil surface (7 cm^2) was cleaned by Ar^+ etching as described elsewhere [41]. The preparation regime and the amount of the Pd deposited were the same as in the case of the Pd–Ti^{3+}-$\square_O/TiO_2$ sample prepared under the XPS and hydrogen TDS control. A low-pressure Hg lamp with a set of interference filters was used as a photon source in photodesorption studies. The flux intensity with $h\nu > 3$ eV through the optical quartz window to the sample was 4×10^{15} cm^{-2} s^{-1}. The exposure of oxygen isotopes to the Ti^{3+}-$\square_O/TiO_2$ surface at 100 K produced only molecular oxygen O_{2ads} and $O^{\delta-}_{2ads}$ states, which was confirmed by TDS and PhDS.

3. Detection of surface intermediates

3.1. Oxygen and hydrogen adsorption: HREELS, TDS

Based on the HREELS data (Fig. 2a), an adsorption of 1.8 Langmuirs (1 L = 1.33×10^{-6} mbar s) of O_2 on Pt(1 1 1) at 105 K results in formation of peroxide O^{2-}_{2ads} molecular species with frequency ν(O–O) bands at 690, 870 cm^{-1} and ν(Pt–O_2) band at 380 cm^{-1} according to [57]. With increasing exposure up to 6 L a frequency of superoxide O^{-}_{2ads} species with ν(O–O) band at 1240 cm^{-1} is observed. Adsorption at 105 K is accompanied by formation of atomic oxygen O_{ads} species with a frequency of ν(Pt–O) band at 460 cm^{-1}. Heating up to 135 K of a layer adsorbed at 105 K causes the transition of molecular oxygen to an atomic state: a sharp increase of the intensity of the band at 460 cm^{-1} is observed (Fig. 2b) [57]. Based on the TDS data, a partial desorption of O_{2ads} to a gas phase proceeds simultaneously with dissociation.

According to HREELS data, the oxygen adsorption at 90 K on the reconstructed Pt(1 0 0)-(hex) surface results in formation of molecular peroxide O^{2-}_{2ads} state with bond axis parallel to the surface and characterized by ν(O–O) band at 940 cm^{-1} (Fig. 3a) [58]. TD-spectra obtained from O_{2ads} adlayer indicate that all oxygen desorbs molecularly at 150 K and therefore spectra do not allow the dissociation of the peroxide O^{2-}_{2ads} molecular species (Fig. 3b). Opposite to Pt(1 0 0)-(hex), heating the molecular oxygen layer on the Pt(1 0 0)-(1 × 1) surface from 90 K up to 200 K is accompanied by dissociation of O^{2-}_{2ads} state with formation of oxygen adatoms O_{ads}, characterized by ν(Pt–O) band at 460 cm^{-1}. According to TDS data, a partial O_2 desorption occurs simultaneously with dissociation at 160 K.

The packing density of the reconstructed Pt(1 0 0)-(hex) surface is known to be higher by 20% than that of the non-reconstructed Pt(1 0 0)-(1 × 1) surface and, according to [59], the Pt(1 0 0)-(hex) → (1 × 1) phase transition induced by hydrogen adsorption causes the excess Pt atoms to be ejected over the upper layer of the metal. After this, O^{2-}_{2ads} can dissociate on the active centers of the (1 × 1) phase, and the $H_{ads} + O_{ads} \rightarrow H_2O_{gas}$ reaction can occur. Fig. 3c shows that interaction of an atomic hydrogen layer (H/Pt(1 0 0)-(hex)) with oxygen (30 L) at 220 K is accompanied by the formation of an oxygen adatom layer with Pt–O bond vibration frequencies of 460, 680 and 920 cm^{-1} [45]. The band at 460 cm^{-1} represents ν(Pt–O) stretching of adsorbed atomic oxygen as a result of oxygen-hydrogen reaction on the (1 0 0)-(1 × 1)-terrace sites. In agreement with O_2/Pt(3 2 1) [60] the bands at 680 and 920 cm^{-1} are intrinsic to atomic states of oxygen on the structural defects (presumably like steps or kinks) induced by the O + H reaction and can be used as a good spectral indicator of the strong structural transformation of the Pt(1 0 0)-(hex) to the Pt(1 0 0)-

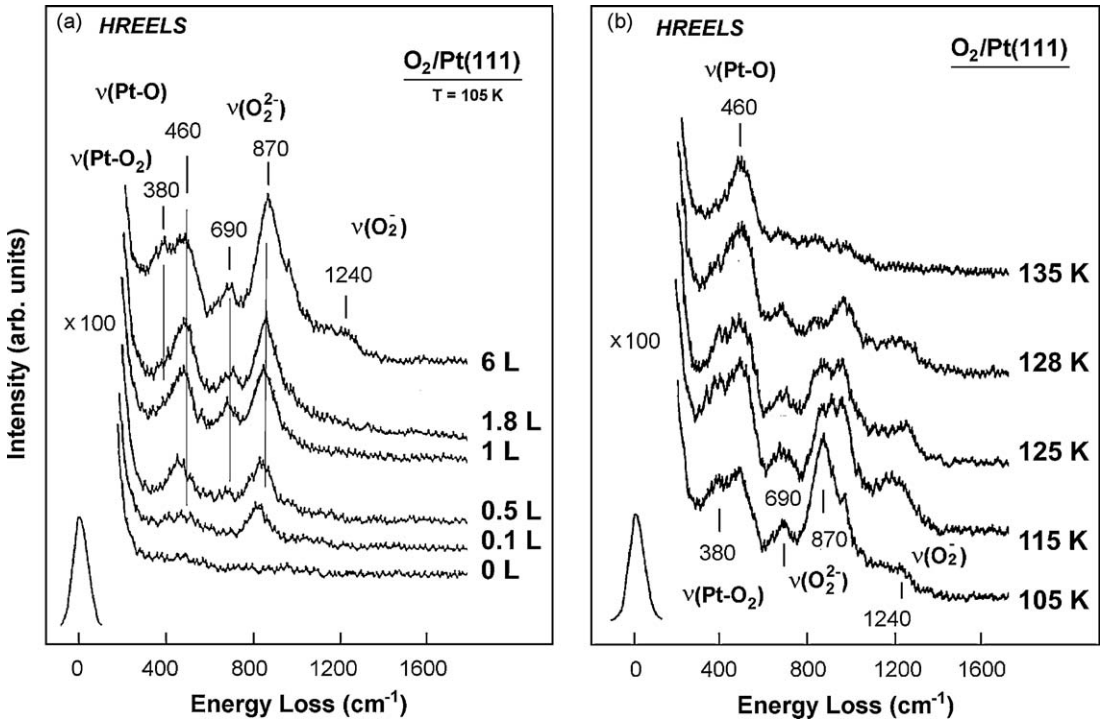

Fig. 2. HREEL spectrum obtained after a 0.1–6 L O_2 exposure on the Pt(1 1 1) surface at 105 K (a) and subsequent (O_{2ads}, 6 L) heating in vacuum up to 135 K (b).

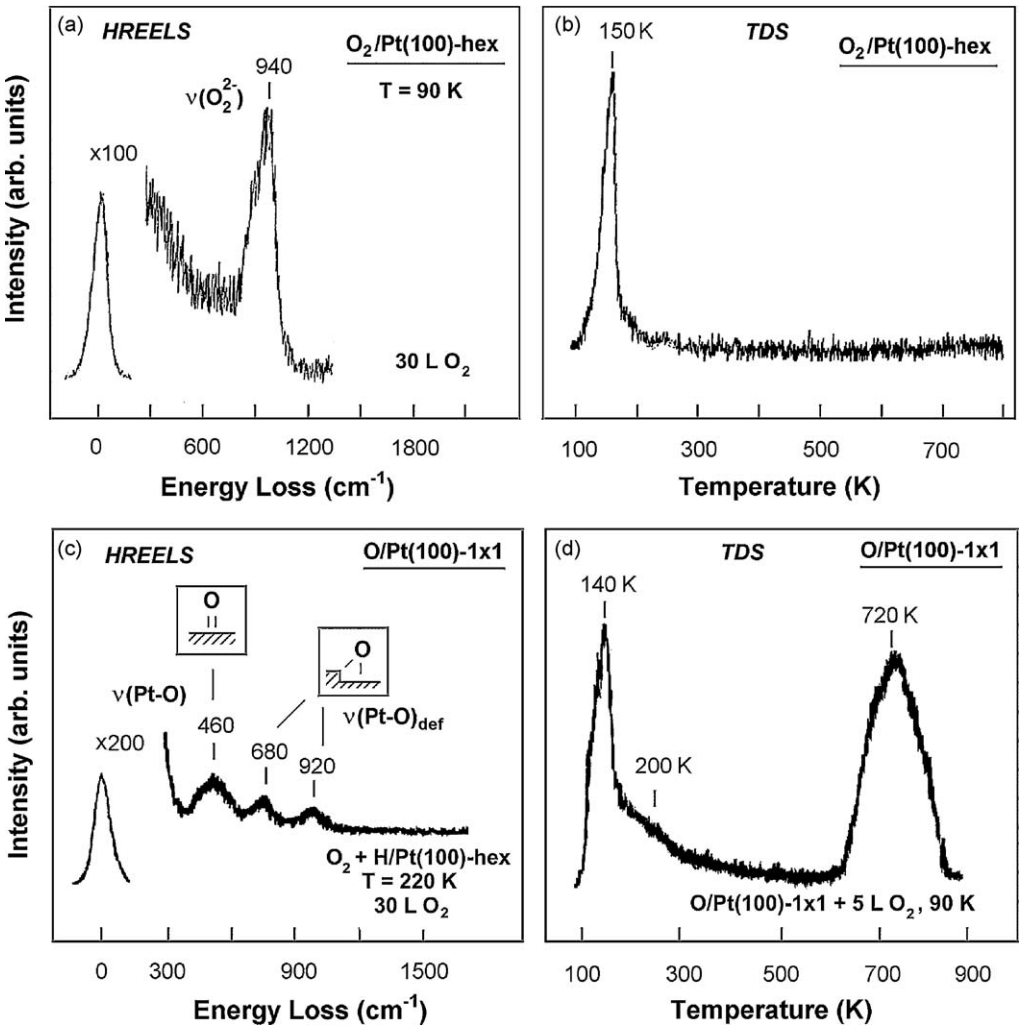

Fig. 3. (a) HREEL spectrum obtained after 30 L O_2 adsorption at 90 K on the Pt(1 0 0)-(hex) surface. (b) TDS spectra from the adsorbed molecular oxygen prepared in (a). (c) HREEL spectrum for the atomic oxygen appearing in the course of 220 K H_{ads} titration by oxygen (30 L) on the H/Pt(1 0 0)-(hex) surface. (d) Resulting O_2 TDS spectrum obtained after 5 L O_2 adsorption at 90 K on a O/Pt(1 0 0)-(1 × 1) surface [45].

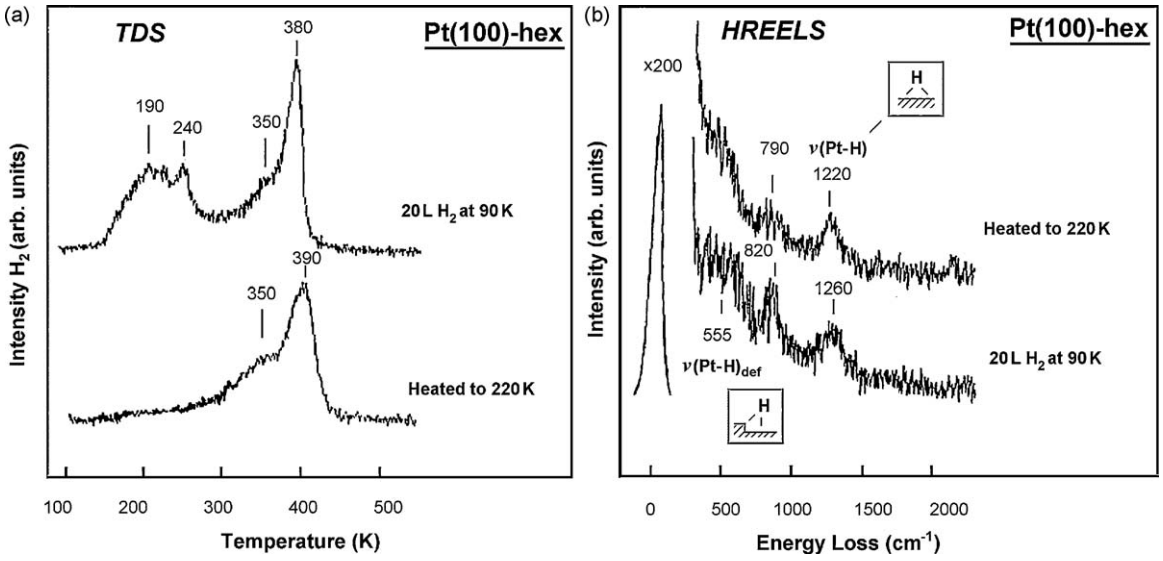

Fig. 4. (a) Hydrogen TD-spectra obtained after an exposure of a 20 L H_2 on the Pt(1 0 0)-(hex) surface at 90 K and subsequent heating in vacuum up to 220 K. (b) HREEL spectra obtained after a 20 L H_2 exposure on the Pt(1 0 0)-(hex) surface at 90 K and subsequent heating in vacuum up to 220 K [45].

Table 1
The vibrational frequencies (in cm^{-1}) of the OH_{ads}-groups on Pt(1 1 1).

Adlayer	T, K	ν(Pt–O)	ν(Pt–OH)	δ(OH)	ν(OH)	Ref.
H_2O dissociation						
$H_2O + * \rightarrow H_2O_{ads}$	100				3420	[18]
$H_2O + O_{ads} \rightarrow OH_{ads} + OH_{ads}$	155	490	430	1015	3480	[18]
$H_2O + O_{ads} \rightarrow OH_{ads} + OH_{ads}$	160		430	820, 1020	3470	[66]
$H_2O_{ads} + h\nu \rightarrow OH_{ads} + H_{ads}$	85		425	825, 1015	3460	[66]
$H_2O + O_{ads} \rightarrow OH_{ads} + OH_{ads}$	155	475	435	820, 915, 1025	3475	[70]
$H_{ads} + O_{ads}$ reaction						
$H_{ads} + O_{ads} \rightarrow OH_{ads}$	135	470		790		[9]
$H_{ads} + O_{ads} \rightarrow OH_{ads}$	150	465		965		[11]
$H_{ads} + O_{ads} \rightarrow OH_{ads}$	146	475		735, 855, 1025		[70]
$H_{ads} + O_{ads} \rightarrow OH_{ads}$	133	475	435	855, 1025		[14]
$H_{ads} + O_{ads} \rightarrow OH_{ads}$	105	460	435	775	3580	[12]

1 meV = 8.06548 cm^{-1}.

(1 × 1) surface. The TD-spectra obtained from the low temperature (O_{ads} + O_{2ads}) layer show the formation of two O_2 desorption peaks at 140 and 200 K, which is accompanied by oxygen desorption peak from the atomic state at 720 K (Fig. 3d). The high temperature oxygen peak is seen due to recombination of O_{ads} surface atoms. Comparable TDS results were found after exposure to O_2 at high temperature (575 K, 3×10^5 L) on Pt(1 0 0)-(hex): two desorption peaks at 660 and 710 K have been observed. If O_2 is adsorbed at 300 K on the clean non-reconstructed Pt(1 0 0)-(1 × 1) surface (prepared by the method proposed by Bonzel et al. [61]) an atomic oxygen states with ν(Pt–O) bands at 540 and 970 cm^{-1} are formed.

At 300 K no hydrogen could be adsorbed on the reconstructed Pt(1 0 0)-(hex) surface [62]. At $T < 300$ K H_2 adsorption leads to characteristic changes in the surface structure: the (hex) → (1 × 1) reverse-reconstruction is observed. However, it has been established that the obtained H/(1 × 1)-like structure does not constitute a perfect (1 × 1) phase, since it contains a certain concentration of structural defects and residual (hex) patches remain as well on the surface [59]. Fig. 4a shows the TD spectrum of hydrogen adsorbed on the (hex)-surface at 90 K. The H_2 spectrum after 20 L exposure is similar to those published in literature [63]: four peaks are easily recognized at 190, 240, 350 and 380 K. After heating up to 220 K the two low-temperature peaks disappeared. The loss spectrum of hydrogen at 90 K exhibits three bands at 555, 820 and 1260 cm^{-1} (Fig. 4b). Annealing at 220 K leads to a decrease in intensity of the two low-frequency bands. According to our study reported in ref. [62] the low-temperature desorption peaks (190 K, 240 K) which are related to the two low-frequency bands at 555 and 820 cm^{-1}, result due to the population of the residual (hex) patches and defects created in the course of the (hex) → (1 × 1) phase transition. The concentration of the defect sites and (hex) patches for saturated H_{ads} layer at 90 K (ca. 1.2 ML) corresponds to ca. 20% of the total hydrogen layer. It has been proposed that the bands at 555 and 1260 cm^{-1} are associated with the bridge H_{ads} state [62].

3.2. OH-groups: HREELS

Two independent routes of the H_2O formation are considered on the platinum metals with participation of hydroxyl groups: successive addition of hydrogen to oxygen atoms ($H_{ads} + O_{ads} \rightarrow OH_{ads}$; $OH_{ads} + H_{ads} \rightarrow H_2O_{ads}$), and the disproportionation reaction ($2OH_{ads} \rightarrow H_2O_{ads} + O_{ads}$) [9,10,26,64]. At studying the mechanism of low temperature H_2 oxidation on the Pt(1 1 1) surface, the following results have been obtained: the reaction effectively proceeds at $T < 150$ K [9,11]; hydrogen adsorption on the vacant centers in oxygen adsorbed layer on the platinum surface is dissociative [65]; H_2O adsorption is molecular on a clean surface, but proceeds with dissociation ($H_2O_{ads} + O_{ads} \rightarrow 2OH_{ads}$) on the oxygen layer ($O_{ads}$/Pt) [18,64,66]; the formation of OH-groups is a result of the H_{ads} and O_{ads} interaction [9,11]. Hence, detection of the intermediate, hydroxyl groups, during the reaction has been the subject of theoretical and experimental investigations. The HREELS evidence for the formation of OH-groups is based on occurrence of deformation vibrations δ(Pt–OH) at 790 cm^{-1} [9] or, on other data [11], their occurrence has been observed at 970 cm^{-1}. Attention is drawn to the missing of those frequencies of stretching vibrations ν(OH) for adsorbed OH-groups in these studies [9,11,14,67] (Table 1).

In our HREELS study, special attention was given to vacuum conditions of the O_{ads} + H_{ads} experiments ($P_{res} < 3 \times 10^{-11}$ mbar), excluding the low temperature H_2O adsorption on the Pt(1 1 1) surface from residual gas. According to [68] the hydrogen layer on Pt(1 1 1) is characterized by the frequencies of stretching vibrations ν(Pt–H) at 500 and 1200 cm^{-1}. A precovered atomic oxygen layer with $\theta = 0.25$ ML (1 ML = Pt surface atoms density = 1.5×10^{15} atoms cm^{-2}) in the structure $p(2 \times 2)$ was carried out by a technique [69]. According to HREELS data, oxygen adsorption on Pt(1 1 1) at 105 K results in formation of two molecular species (Fig. 2a). Heating up to 250 K causes the transition of molecular oxygen to an atomic state characterized by a frequency of ν(Pt–O) band at 460 cm^{-1} (Fig. 5). The proposed technique allows one to keep a high concentration of the empty sites, which is necessary for subsequent dissociation of H_2 on a O/Pt(1 1 1) surface. Fig. 5 shows that interaction of an atomic oxygen

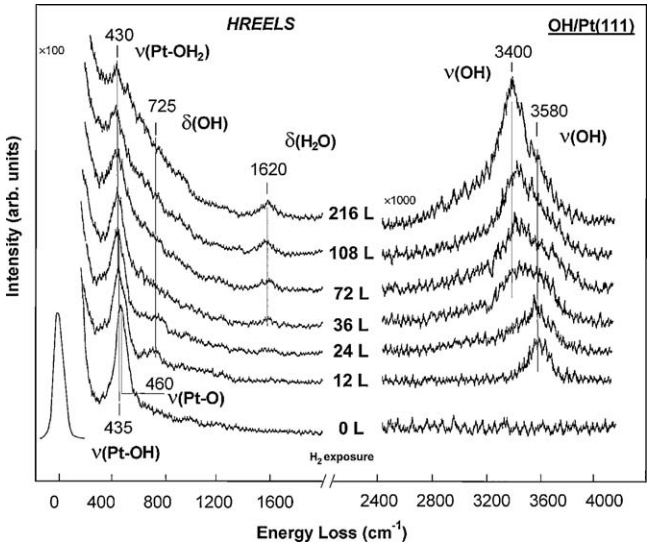

Fig. 5. HREEL-spectra obtained for stepwise titrating H_2 to the Pt(1 1 1)-O surface ($\theta = 0.25$ ML) at 105 K to an accumulated dose of 216 L H_2. The accumulated H_2 dose is indicated for each spectrum [12].

Table 2
DFT results for equilibrium heights (r_0) above the surface, bond length (d_0), vibration frequencies (ν = stretch, δ = bend) of adsorbed H, O atoms and OH, H_2O molecules for following adsorption sites on Pt(1 1 1) at θ = 0.25 ML.

Adlayer	Adsorption site	Equilibrium height r_0 (Å)	Bond length d_0 (Å)	Vibration frequencies $\nu_\perp$ (cm^{-1})	Vibration frequencies δ(OH) (cm^{-1})	Vibration frequencies ν(OH) (cm^{-1})
H/Pt(1 1 1)	fcc	0.97		1218		
O/Pt(1 1 1)	fcc	1.23		499		
OH/Pt(1 1 1)	Bridge	1.71	0.97	427	1310	3615
H_2O/Pt(1 1 1)	On-top	2.26	0.97	265		

layer with hydrogen (105 K, 12–24 L) in the initial step of $H_{ads} + O_{ads} \rightarrow OH_{ads}$ reaction is accompanied by the formation of the hydroxyl groups with the frequencies of stretching vibrations ν(O–H) at 3580 cm^{-1} and deformation vibrations δ(Pt–OH) at 775 cm^{-1} [12]. In the second step of $H_{ads} + OH_{ads} \rightarrow H_2O_{ads}$ reaction (36–72 L H_2), the formation of H_2O_{ads} layer occurs with the frequencies of deformation vibrations δ(HOH) at 1620 cm^{-1}. Simultaneously the high-frequency area ν(O–H) is accompanied by displacement on 180 cm^{-1} up to value of 3400 cm^{-1} that is responsible for H_2O_{ads} layer. Disappearance of deformation vibrations δ(Pt–OH) at 775 cm^{-1} is also observed. At H_2 exposure 108–216 L practically all pre-adsorbed oxygen layer turns to H_2O_{ads} layer. The band at 430 cm^{-1} represents ν(Pt–OH_2) stretching vibrations of adsorbed water molecules. The *S*-shaped character of intensity vibrations δ(HOH) suggests that the reaction $H_{ads} + O_{ads} \rightarrow OH_{ads} + H_{ads} \rightarrow H_2O_{ads}$ should be proportional to borderline of oxygen islands O_{ads}. The existence of small oxygen islands has been seen during O_2 adsorption on Pt(1 1 1) by STM [70]. Direct evidence for the existence of islands during the reaction has been obtained from our FEM studies on Pt, Ir [27], Rh [28] and PEEM on Pt(1 0 0) [22].

A comparison between loss frequencies for H_2O adsorbed on the clean and oxygen-precovered Pt(1 1 1) surfaces [18,66,67] and for the $H_2 + O_{ads}$ reaction [9,11,12,14,67] proceeding at 105–160 K are presented in Table 1. As one can see from the tabulated data, H_2O molecules dissociation on the O/Pt(1 1 1) surface is characterized by the following vibrational frequencies for OH_{ads}-groups: δ(OH) = 825–1025 cm^{-1}, ν(OH) = 3460–3480 cm^{-1}. As water molecules do not dissociate on the clean surface, the deformation band δ(OH) of the hydroxyl OH_{ads} is absent in the spectrum of H_2O_{ads}/Pt(1 1 1): ν(Pt–OH_2) = 550 cm^{-1}, δ(HOH) = 1620 cm^{-1}, ν(OH) = 3400 cm^{-1}. The difference is observed in the frequencies of the stretching ν(OH) as well: the OH_{ads} reveals the high value of 3480 cm^{-1} as compared to that of H_2O_{ads} adlayer (3400 cm^{-1}). The authors of [9] have succeeded in finding the step of the OH_{ads} formation in the $H_2 + O_{ads}$ reaction at 135 K (the loss peak at 790 cm^{-1}) while the reaction rate was so high at 150 K that H_2O_{ads} production (ν(Pt–OH_2) = 590 cm^{-1}, δ(HOH) = 1630 cm^{-1}) along with OH_{ads} formation has been already observed at the initial stage [11]. It is clear that the temperature decrease makes it possible to study the reaction steps $H_2 + O_{ads} \rightarrow OH_{ads} \rightarrow H_2O_{ads}$ separately [12]. In accordance with our investigation performed by FEM [5] the $H_2 + O_{ads}$ reaction could be initiated at 100 K on the stepped platinum planes of (3 3 1) type.

In our study two steps of the $H_2 + O_{ads}$ reaction at 105 K have been reliably discerned:

1st step: $H_{ads} + O_{ads} \rightarrow OH_{ads}$ is accompanied by the appearance of the vibrational bands of the OH_{ads} species: ν(Pt–OH) = 435 cm^{-1}, δ(OH) = 775 cm^{-1}, ν(OH) = 3580 cm^{-1} (Table 1).
2nd step: $H_{ads} + OH_{ads} \rightarrow H_2O_{ads}$ is accompanied by the disappearance of the OH_{ads} deformations and the appearance of the vibrational bands from the H_2O_{ads} adlayer: ν(Pt–OH_2) = 430 cm^{-1}, δ(HOH) = 1620 cm^{-1}, ν(OH) = 3400 cm^{-1} (Fig. 5).

The appearance of OH-hydroxyl groups during the initial 1st step of $H_{ads} + O_{ads}$ reaction is a direct evidence for the LH-mechanism involving sequential addition of hydrogen atoms to adsorbed oxygen. We suppose that the isolated OH_{ads}-groups are produced in the course of the 1st step of the reaction as far as the ν(OH) stretching frequency is equal to 3580 cm^{-1} and is located between the values for H_2O molecule in the adsorbed (3400 cm^{-1}) and gaseous (3700 cm^{-1}) states. Moreover, just this region of the stretchings is typical only of the hydroxyl-related spectra on the metal surfaces, for example: ν(OH) = 3560 cm^{-1} on Ni(1 1 0) [71] and ν(OH) = 3640 cm^{-1} on Ag(1 1 1) [72].

In this connection it should be noted that there still remain some questions concerning the kinetics of the water formation for $OH_{ads} + H_{ads} \rightarrow H_2O_{ads}$ and $2OH_{ads} \rightarrow H_2O_{ads} + O_{ads}$ reactions. According to TPR studies on the Pt(1 1 1) surface [66], the $OH_{ads} + H_{ads}$ route should be faster (H_2O desorption at 180 K) than the $OH_{ads} + OH_{ads}$ route (H_2O desorption at 215 K), at least at low temperatures. However, at large oxygen coverage the $OH_{ads} + OH_{ads}$ reaction may become more important [19].

3.3. OH-groups: DFT

Theoretical calculations [73] were performed to evaluate our observed vibrational modes based on a density functional theory (DFT). The nature of the reaction intermediate (H_{ads}, O_{ads}, OH_{ads}, H_2O_{ads}) on Pt(1 1 1) has been studied by DFT within the local density approximation (LDA). The simulations were conducted using ADF2003-BAND and ESPRESSO-3.1 programs. We present here the calculated value of equilibrium heights above the surface, bond length and vibration frequencies (Table 2). We have employed a three-layer slab for simulation of the Pt(1 1 1) surface (Fig. 6a). It is known that adsorption of oxygen on Pt(1 1 1) at coverage of 0.25 ML corresponds to a surface $p(2 \times 2)$ atomic oxygen structure [11] where there is only one oxygen atom per unit cell. Adsorbed H, O atoms and OH, H_2O molecules can occupy the following states: two threefold hollow sites, namely the fcc and hcp, twofold bridge site and on-top, using only adsorbed species per unit cell (Fig. 6a). The geometries of the adsorbed OH and H_2O species are optimized.

Four different sites were analyzed and it was found that the most energetically favorable are threefold hollow sites (fcc and hcp) in coordination Pt_3–O_{ads} and Pt_3–H_{ads} as compared to weakly bond energy on-top or bridge sites. Computed frequencies of symmetrical valence vibrations of H_{ads} and O_{ads} atoms occurring perpendicular to the surface heavily depend on the number of metal atoms coordinating with the adsorbed atom. Vibration frequency dramatically increases with decreasing the number of bonds in adsorption center [74]. The bonding configuration (bridge site) and the vibrational normal modes for a surface OH-groups are shown in Fig. 6b and c. The ν(Pt–OH) stretching mode at 427 and δ(OH) bending mode at 1310 cm^{-1} was calculated on bridge sites (Table 2). The ν(OH) stretching mode was calculated to be at 3615 cm^{-1} according to the similar frequency experimental value 3580 cm^{-1} (Fig. 5). A tilt ($\alpha^0 = 17^\circ$) from the bridge site toward the surface plane, the

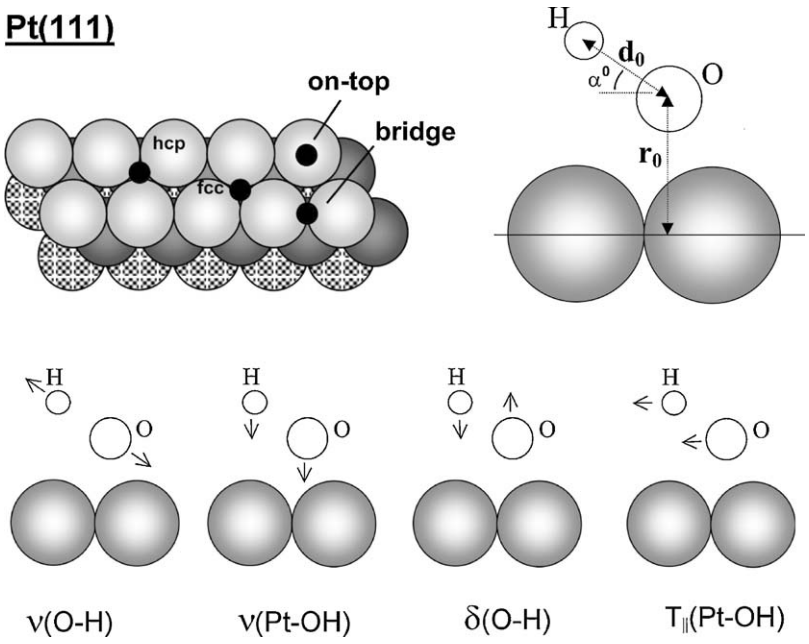

Fig. 6. (a) Schematic top view of the Pt(1 1 1) surface: adsorption sites of H, O atoms and OH, H_2O molecules. (b) Side view of the tilted geometry of OH_{ads}-group on Pt(1 1 1) at the bridge site: bond lengths (r_0, d_0) and angles of an inclination (α^0). (c) Schematic vibrations of the normal modes of OH_{ads}-groups on Pt(1 1 1).

equilibrium height of the O atom above the center of Pt atoms and the O–H bond length were calculated on the bridge sites with average values of 1.71 and 0.97 Å, respectively (Table 2). Calculations at 0.25 ML coverage show that OH on the bridge sites is more stable than that on the hollow sites or on-top. The H_2O_{ads} on Pt(1 1 1) has the equilibrium height of 2.26 Å, the O–H bond length of 0.97 Å (Table 2), and it prefers the on-top site with the intramolecular H–O–H bond angle value of 108° that is almost identical to that in the H_2O molecule. Our calculated vibrational frequencies for OH-groups are similar to the recent DFT results on the Pt(1 1 1) surface [75,76].

In Fig. 7 we show a transition state geometry for H_2O formation from adsorbed O-atoms during the consecutive connection of H-atoms. The appearance of OH-hydroxyl groups during the initial 1st step of $H_{ads} + O_{ads}$ reaction is accompanied by transition of oxygen atom from the hollow site (Pt_3-O_{ads}) into bridge site Pt_2-$(OH)_{ads}$. Water formation in the 2nd step of $OH_{ads} + H_{ads} \rightarrow H_2O_{ads}$ reaction is characterized by the subsequent transition of oxygen atom from the bridge site (Pt_2-$(OH)_{ads}$) into on-top site (Pt_1-$(OH_2)_{ads}$) that is accompanied by cleaning of the centers active in H_2 and O_2 dissociation.

3.4. Summary

The low temperature adsorption and reaction between hydrogen and oxygen on the Pt(1 1 1), Pt(1 0 0)-(hex), Pt(1 0 0)-(1 × 1) surfaces were investigated using experimental (HREELS, TPR) and theoretical (DFT) tools to learn the details of the reaction dynamics on these catalytic surfaces. The key results from our studies are summarized below.

Both Pt(1 1 1) and Pt(1 0 0)-(1 × 1) surfaces are catalytically active for the H_2 oxidation due to their ability to dissociate O_2 and H_2 molecules. Results from $H_2 + O_{ads}$ titrating experiments directly support the conclusion that OH-hydroxyls are the intermediate species which react with hydrogen atoms at low temperature (105 K) to form H_2O. An interesting feature of OH formation is evidence that the reaction takes place at the boundaries of the O_{ads} islands. A remarkable result is the observation in $H_{ads} + O_{ads} \rightarrow OH_{ads}$ reaction of a new ν(OH) stretching frequency at 3580 cm^{-1} that is typical only of the isolated hydroxyl-related spectra. The L–H detailed mechanism involves the formation of OH-species (slow 1st step) and its reaction with hydrogen to form water (fast 2nd step). The H_2O formation is accompanied by transition of oxygen atom from the hollow site (Pt_3-O_{ads}) to bridge site Pt_2-$(OH)_{ads}$ and finally, to on-top site (Pt_1-$(OH_2)_{ads}$) that is accompanied by cleaning of the catalytic centers active in hydrogen and oxygen dissociation.

4. Chemical waves in catalytic H_2 oxidation

4.1. Surface reconstruction of Pt(1 0 0)-(hex) ↔ (1 × 1): Pt-tip study of $H_2 + O_{ads}$ titration reaction

Since the first discovery of a correlation between reconstruction and kinetic oscillations in CO oxidation on the Pt(1 0 0) single crystal by Ertl et al. [77], this surface has become one of the most

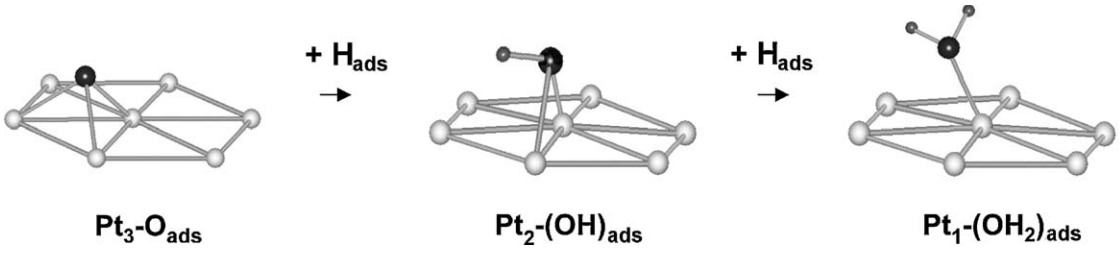

Fig. 7. Transition state geometry for H_2O formation from adsorbed O and H atoms on Pt(1 1 1).

extensively investigated oscillatory system in heterogeneous catalysis. The reconstructed Pt(1 0 0)-(hex) surface has a compressed top layer in which the packing atom density is 20% higher than that of the non-reconstructed Pt(1 0 0)-(1 × 1) surface. The reaction mechanism leading to the oscillatory behavior is associated with periodic phase transition of the surface (hex) ↔ (1 × 1) induced by adsorbed CO or H_2 dissociative adsorption [78]. The atomic density of the (1 × 1) surface is 1.28×10^{15} Pt atoms cm^{-2} [78]. This is approximately 25% lower than the atomic density of the (hex) phase (i.e., 1.61×10^{15} Pt atoms cm^{-2}) [79]. This density difference results in significant mass transport of platinum atoms during the back-reconstruction and causes the excess Pt atoms to be ejected out over the layer of the metal. STM data demonstrate [79–81] that expelled platinum atoms formed the clusters with size of ca. 15–25 Å. The hydrogen-adsorption-induced reconstruction (hex) involves the movement of ca. 1.3×10^{15} Pt atoms cm^{-2} to their expected (1 × 1) bulk-like locations [78]. This is accompanied by an increase in the oxygen sticking coefficient from $\approx 10^{-3}$ (hex) to $\approx 10^{-1}$ (1 × 1), thus inducing a transition from a catalytically inactive state into an active state with a high oxygen sticking coefficient.

The Pt(1 0 0)-*nano*plane reconstruction was the first reported for the Pt-tip surface by means of FIM investigation. The (1 0 0)-(1 × 1) surface of Pt was prepared by low temperature field evaporation of the Pt(1 0 0)-oriented tip at 78 K [82]. The FIM observation showed that the clean (1 0 0)-(1 × 1) surface was metastable and transformed thermally activated back into the (hex)-phase above 270 K [83]. For comparison, the clean Pt(1 0 0)-(1 × 1) single crystal surface was found to reconstruct into (hex) at $T \sim 400$ K [84,85].

In our study the interaction of hydrogen with pre-adsorbed oxygen layer was investigated at two temperatures: at 395 K on the (1 0 0)-(hex)-oriented Pt-tip (Fig. 8a) and 300 K on the (1 0 0)-(1 × 1)-oriented Pt-tip (Fig. 8f) using a hydrogen pressure of 4.6×10^{-7} mbar. Fig. 8 presents the FEM images of the catalytic titration reaction $H_{2gas} + O_{ads} \rightarrow H_2O_{gas} + H_{ads}$. In the experiments described in this section, the oxygen layer was produced by adsorption of oxygen at exposure ca. 10^3 L followed by pumping. The work function increases to the value typical of the oxygen adlayer ($\Delta\varphi \approx 1.1$ eV). Sequence of FEM images demonstrates how the oxygen precovered surface being transformed into hydrogen adsorbed layer ($\Delta\varphi \approx 0.2$ eV). The interpretation of the FEM images changes is facilitated by the fact that reaction of oxygen with hydrogen results in a marked work function decrease and, consequently, an increase in electron emission. In Fig. 8b–e the sequence of FEM images on the (1 0 0)-(hex)-oriented Pt-tip (a) shows that the oxygen layer reacts with H_2 via a reaction front in a face-specific reaction sequence starting (at $\tau = 0$) on the stepped (3 3 1) regions around the (1 1 1) plane (bright areas in Fig. 8b) and ending (after 1.4 s) on the (1 0 0) apex plane (Fig. 8e). In these regions the isolated oxygen islands still persist after 1.4 s (Fig. 8e). In Fig. 8g–j the sequence of FEM images on the (1 0 0)-(1 × 1)-oriented Pt-tip (f) shows the dark O_{ads}-layer (g) being transformed into a bright H_{ads}-layer (h–j) via a reaction front in a face-specific reaction sequence starting (at $\tau = 0$) on the central (1 0 0)-(1 × 1) plane (g) and ending (after 9.6 s) on the (1 1 2), (3 1 0) planes (j). One can see that the (1 0 0)-(1 × 1) surface has a very high reactivity. The hydrogen islands increase in size and after about 10 s all the oxygen layer has disappeared (Fig. 8h–j). From the sequence in images the following order in reactivity of adsorbed oxygen is observed: (i) (1 0 0)-(hex)-oriented Pt-tip: oxygen on $(1\,1\,1)_{step}$ and (3 3 1) > (112) > (2 1 0), (3 1 0) > (1 0 0)-(hex); (ii) (1 0 0)-(1 × 1)-oriented Pt-tip: oxygen on (1 0 0)-(1 × 1) > (1 1 2) > (3 1 0) > (2 1 0).

With reversed polarity, taken $F_{FIM} = 1.5$ V/Å, field ion current (H_2O^+/H_3O^+) could be measured by field ion microscopy [55]. After the introduction of hydrogen the ion current rises immediately and forms FIM images of the catalytic titration reaction $H_{2gas} + O_{ads} \rightarrow H_2O_{gas} + H_{ads}$ (Fig. 9). The reaction exhibits similar features both on Pt tips in FEM (Fig. 8b–e) and FIM (Fig. 9) studies. The reaction starts on the stepped regions (3 3 1) and around the (1 1 1) planes. This agrees well with the pronounced catalytic activity of the stepped platinum surfaces in the hydrogenation reaction, where the steps represent the trapping centers for hydrogen dissociative adsorption [86,87]. Subsequently the *narrow* reaction zone moves in the direction from (1 1 1) towards the (1 0 0) plane via stepped regions of the type (1 1 2) and (1 1 3) ($\tau = 1.6$ s). Than the reaction of hydrogen with oxygen on the atomically rough (2 1 0), (3 1 0) planes has been completed ($\tau = 1.72$ s), the reaction zone moves towards the (1 0 0)-(hex) plane. Oxygen adsorbed on this plane is the least reactive one ($\tau = 1.88$ s). During our first FIM

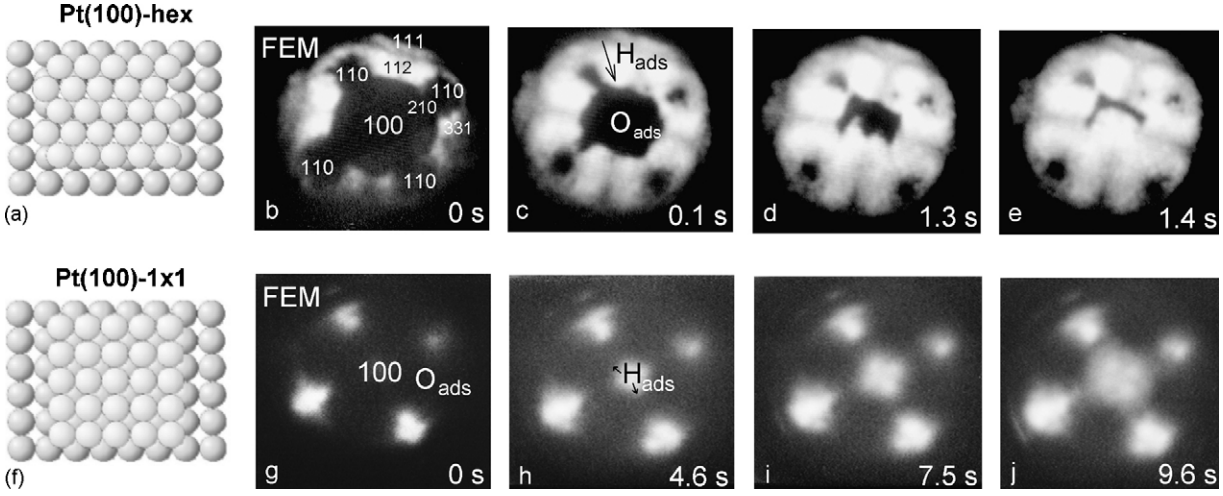

Fig. 8. Plan view of the (1 0 0) oriented Pt-tip shows the atomic structure on the (1 0 0)-(hex) (a) and (1 0 0)-(1 × 1) (f) apex surfaces. Comparison of the FEM images showing the specificity of individual nanoplanes of platinum tip (1800 Å radius) in the titration reaction of hydrogen adsorbed from the gas phase ($P = 4.6 \times 10^{-7}$ mbar) with the pre-adsorbed oxygen layers: (b) on the surface of the (1 0 0)-(hex) oriented Pt-tip after O_2 adsorption at 300 K, exposure $\sim 10^3$ L, $\Delta\varphi = 1.2$ eV; (g) on the surface of the (1 0 0)-(1 × 1) oriented Pt-tip (prepared by field evaporation at 78 K) after O_2 adsorption at 78 K (10 L) and additional oxygen adsorption at 300 K, ca. 10^3 L, $\Delta\varphi = 1.2$ eV. In FEM the disappearance of the oxygen layer (O_{ads}, black) is characterized by bright-field emission of the hydrogen layer (H_{ads}, bright) at the next temperatures of $H_2 + O_{ads}$ reaction: 395 K, (b–e), Pt(1 0 0)-(hex), time value ~1.4 s; 300 K, (g–j), Pt(1 0 0)-(1 × 1), time value ca. 9.6 s [29].

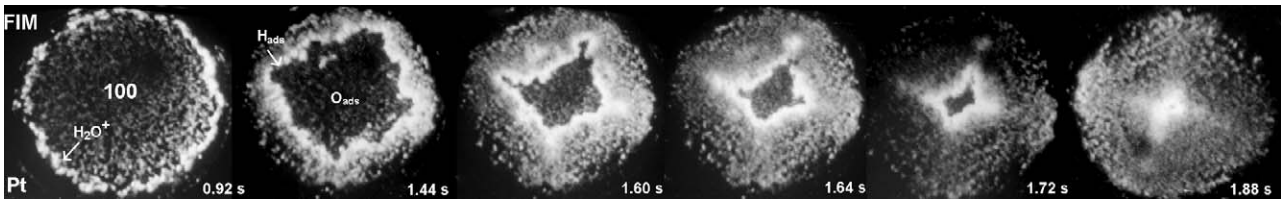

Fig. 9. FIM images of the (1 0 0)-(hex) oriented Pt-tip during the titration reaction of O_{ads} with hydrogen: T = 380 K, $P(H_2) = 4.6 \times 10^{-7}$ mbar, 1800 Å radius, $F \approx 1.5$ V/Å. In FIM a bright reaction front (H_2O^+ ions) is imaged from {3 3 1}, {1 1 1} → {2 1 0} → {1 0 0}; time value ca. 1.9 s.

experiments (H_2O^+-ion production as to be identified in the mini-mass spectrometer), it was assumed that the brighter front is produced by H_2O^+ ions being formed near the tip surface ($X_c \approx 4$ Å) from the desorbing reaction product ($H_2O_{gas} \xrightarrow{field} H_2O^+ + e^-$) [88]. In the subsequent studies it was found that the formation of H_3O^+ ions can also occur during the field-induced surface reaction for a protonation pathway involving H_{ads} and H_2O_{ads}: $H_{ads} + H_2O_{ads} \xrightarrow{field} H_3O^+ + e^- + 2*$ [33,55,89]. In the latter case a field-induced proton transfer of adsorbed hydrogen, H_{ads}, leads to the formation of hydronium ions H_3O^+. When H_2O^+-ion currents (or H_2O^+-image) are given in the following, they will be referring to the sum of H_2O^+/H_3O^+ ion intensities. More details of H_3O^+ ion formation processes are presently analyzed by mass spectrometry and appearance energy spectroscopy [33]. In fact, reversing the polarity of the electric field did not affect the propagation velocities ($\tau_{FEM} \approx \tau_{FIM}$) of chemical waves during the titration reaction of O_{ads} with hydrogen studied by FEM (negative field, $F \approx 0.4$ V/Å, Fig. 8b–e) and FIM (positive field, $F \approx 1.5$ V/Å, Fig. 9). From point of view [33] the field-induced routes are very fast in comparison with chemical steps such as the adsorption process and the intermediates formation. Hence, in a unique fashion the temporarily catalytically active sites could be identified as at a field free condition.

An important FIM feature of the catalytic titration reaction $H_{2\ gas} + O_{ads} \rightarrow H_2O_{gas} + H_{ads}$ on platinum is the occurrence of the sharp reaction zone boundary and its propagation in the region of atomically rough surfaces: on the (3 1 0) and (2 1 0) planes. This mobile sharp boundary suggests that this reaction concerns an extremely narrow surface region ca. 30 Å, within the limits of the FIM resolution (ca. 5 Å).

4.2. Self-sustained oscillations: surface waves

The rate of $H_2 + O_2$ reaction depends on three parameters: T, $P(O_2)$ and $P(H_2)$. Fig. 10A shows the rate of reaction for Pt-tip as a function of $P(H_2)$ at constant T and $P(O_2)$. From left to right, three reaction regions can be distinguished: oxygen side (O_{ads}), transition point and hydrogen side (H_{ads}). At different temperatures (300–465 K) and $P(O_2) = 2 \times 10^{-4}$ mbar, the rate of reaction (lg H_2O^+) increases linearly (O_{ads}-side) with $P(H_2)$ up to the transition point ($P(H_2) = 4 \times 10^{-4}$ mbar), where subsequent increase in H_2 pressure makes the reaction rate drop linearly (H_{ads}-side). For all temperatures, the initial rise in the rate remains linear versus $P(H_2)$ and with the same H_2 pressure dependence (same slope) up to the point of transition. The transition point ($\theta_O \rightarrow \theta_H$) occurs in a very narrow range of $P(H_2)$, in which the surface wave appears. Fig. 10B(a–d) demonstrates how chemical waves can develop. At constant oxygen pressure ($P(O_2) = 5 \times 10^{-4}$ mbar) the (1 0 0)-oriented Pt-tip surface is precovered with oxygen layer (Fig. 10B-a). The medium brightness of FIM image is mainly formed by O_2^+ ions (except of upper right corner) that are preferentially field-ionized at O_{ads}-sites of the Pt surface [90]. When hydrogen is introduced to the transition point ($P(H_2) = 6 \times 10^{-4}$ mbar) the reaction front starts at (3 3 1) planes at the top right in (a) and proceeds quickly towards the (1 0 0) plane. During this fast movement the (1 1 0) planes are initially excluded. The anisotropically propagating wave front (very bright regions) moves in the direction from (1 1 0) towards the (1 0 0) plane in 120 ms (b), and finally, after 360 ms (d) a uniform, catalytically active surface is formed. The image brightness of H_2O^+ ions represents surface areas with high turnover frequencies. This means that an active surface for the H_2O production in the transition point

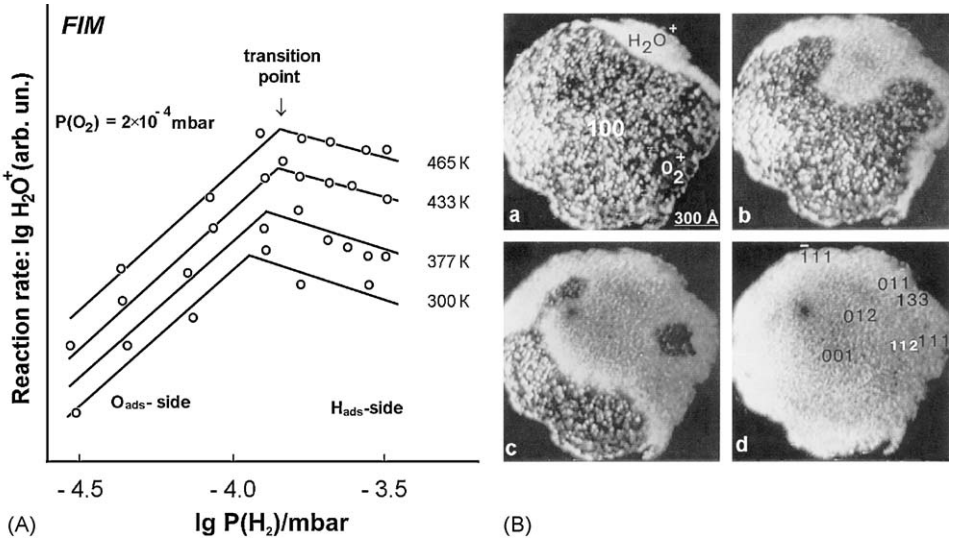

Fig. 10. (A) The rate of reaction (lg H_2O^+) on Pt-tip as a function of $P(H_2)$ for $P(O_2) = 2 \times 10^{-4}$ mbar and different temperatures, tip radius r = 1700 Å, $F \approx 1.5$ V/Å. (B) FIM images (a–d) of $H_2 + O_2$ reaction over O_{ads}-side precovered surface at the transition region: T = 300 K, $P(O_2) = 5 \times 10^{-4}$ mbar, at (a) $\tau = 0$, added $P(H_2) = 6 \times 10^{-4}$ mbar. Images demonstrate initial reaction steps for organizing the self-sustained oscillations. The bright reaction front moves from upper right corner via the planes (3 3 1), (1 1 1) → (2 1 0) → (1 0 0) → (1 1 2), (1 1 3). (a) 0 ms; (b) 120 ms; (c) 150 ms; (d) 360 ms. Medium front propagation rate: 10000 Å × s^{-1} [30].

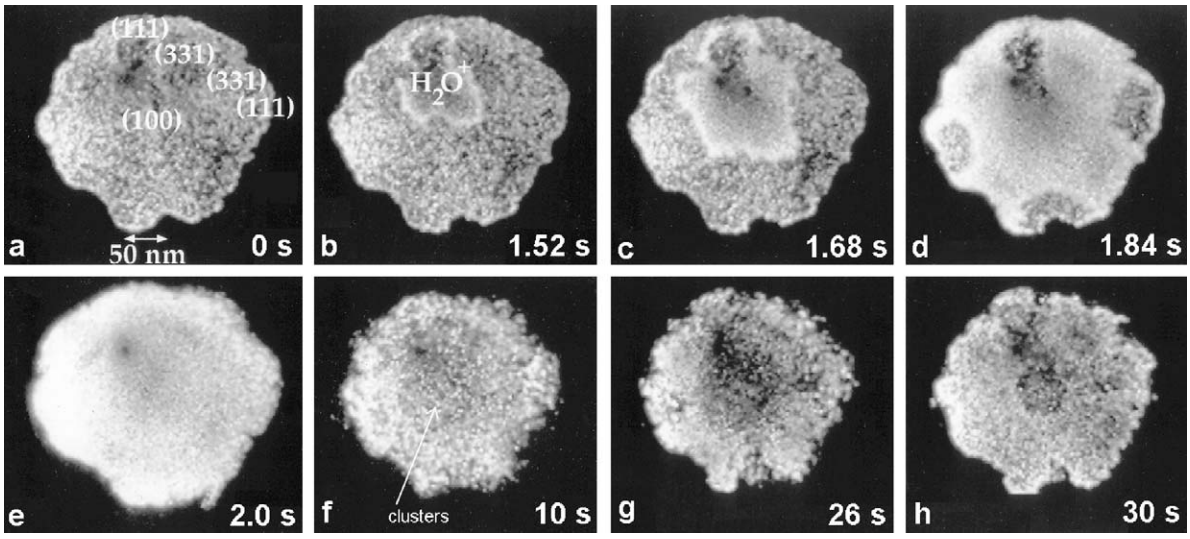

Fig. 11. A sequence of FIM images during the H_2 oxidation at 300 K, $F \approx 1.5$ V/Å. Imaging gases are O_2 (from the reactants) and H_2O formed during the reaction. The time intervals after the initial image ($\tau = 0_s$) are given at the lower right corners of the images [22].

was created after O_{ads} had been partially removed. This is the surface which starts to be covered with H_{ads}, but still has a high sticking coefficient for O_2, such that the $H_2 + O_2$ reaction can proceed. A completely hydrogen-covered surface (H_{ads}-side) has a low sticking probability for oxygen and therefore a decrease of reaction rate for the $H_2 + O_2$ reaction (Fig. 10A).

The imaging situation for H_2 oxidation in steady-state reaction conditions on Pt is even more dramatic because the product of the catalytic reaction, H_2O, acts directly as an imaging gas [22,88]. Molecular water has an ionization potential of $I_{H_2O} = 12.60$ eV in the reaction gas mixture where $I_{O_2} = 12.60$ eV and $I_{H_2} = 15.42$ eV. At 300 K, H_2O, the reaction product of H_2 oxidation, desorbs immediately, in a very short residence time. It was shown that H_2O^+/H_3O^+ ions are the main ionic species, which serve as the imaging gas in the FIM, thus indicating the catalytic active centers of the product formation *in situ* and in real time [55].

Isothermal, non-linear dynamic processes in the $H_2 + O_2$ reaction on the Pt tips have been studied simultaneously with the formation of face-specific adsorption islands and the mobility of reaction/diffusion fronts. The role of the Pt(1 0 0) phase transition will be discussed for data of Fig. 11. In Fig. 11a–h the sequence of *in situ* FIM images at 300 K demonstrates how the chemical waves can develop during the catalytic oxidation of hydrogen [22,88]. The areas with medium brightness represent O_{ads}-layer imaged by O_2^+ ions; very bright regions indicate areas with a high production rate of H_2O; dim areas are covered by H_{ads}. The oscillation cycles start from an O_{ads}-layer (a) that shows the formation of a highly reactive zone yielding H_2O (H_2O^+) product molecules in the central (1 0 0) plane (b). This zone spreads rapidly over the whole surface (c–e), including a Pt(1 0 0)-(1 × 1) surface at this stage. Due to the high reactivity of the Pt(1 0 0)-(1 × 1) surface, the coverages of both reacting species become rather low. As a consequence, the (1 × 1)-surface is no longer stable, but transforms into the hexagonal phase (f). Because the sticking coefficient for O_2 is much lower on the Pt(1 0 0)-(hex) surface, build-up of a H_{ads}-layer takes place resulting in the lifting of the hexagonal reconstruction back to the (1 × 1)-phase (g–h). The transition of the Pt(1 0 0)-(hex) into the Pt(1 0 0)-(1 × 1) surface is combined with a change in the density of the top Pt layer and during this process about 20% of its atoms are ejected [91]. This process is visible *in situ* and manifests itself by the appearance of fluctuating small Pt clusters (brighter spots) that can be discerned in the image (f). The H_{ads} regions still appear dim in the FIM images and shrink in diameter (g–h), until the surface is again completely covered with oxygen as at (a). During this oscillatory behavior, the imaging process has been combined with mass spectrometry and field ion appearance energy spectroscopy measurements [55].

The reconstruction in the (1 0 0) plane represents the sequence:

$$O_{ads}(1 \times 1)Pt \xrightarrow{H_2} H_2O_{gas} + (hex)Pt \xrightarrow{H_2} H_{ads}(1 \times 1)Pt \xrightarrow{O_2} H_2O_{gas} + O_{ads}(1 \times 1)Pt$$

Thus, we can conclude that during oscillations the catalytic reaction creates and destroys its own active centers on the surface of the catalyst. It was found that the Pt(1 0 0) surface switches reversibly from an inactive state (hex) into a highly active state (1 × 1) under CO + O_2 self-oscillation conditions for the Pt-tip surface too [92]. These results demonstrate that the critical size of surface nanoplanes for which rate oscillations and other collective phenomena can be observed is very small. Probably even less than ca. 200 Å size is sufficient for the generation of chemical waves. Recently, using Monte Carlo simulations [93,94], it was predicted that for the disappearance of non-linear phenomena (hysteresis, bistability, oscillations) the nanoplanes must contain less than ca. 100–200 surface sites.

4.3. Summary

Sharp tips of Pt, up to several hundreds Å in size, have been used to perform investigations of dynamic surface processes simultaneously on different crystallographic nanoplanes of the emitter tip. In summary, one can say that the reaction fronts are combined with a reversible transformation of layers ($O_{ads} \leftrightarrow H_{ads}$) in a rather complicated sequence of reaction steps that involve the reaction $O_{ads} \rightarrow H_{ads}$ during oscillations: $O_{ads} \rightarrow OH_{ads} \rightarrow H_2O_{ads} \rightarrow H_2O_{gas}\uparrow \rightarrow$ empty sites + $H_{2gas} \rightarrow H_{ads}$. Islands of O_{ads} or H_{ads} can form in the adsorbed layer and the catalytic reaction then proceeds along the borderlines of these islands. The turnover frequency of this reaction is not directly determined by impingement rates of reactants (H_2, O_2) from the gas phase, but mainly by properties of diffusion/reaction fronts typical of self-sustained oscillations. For the $H_2 + O_2$/Pt system: (i) the observed character of oscillating behavior directly shows the catalytically active sites in the product water molecules (H_2O^+/H_3O^+ ions); (ii) H_{ads}- and O_{ads}-fronts move in reverse directions. The hydrogen-modified Pt(1 0 0)-(hex) surface shows an increase

in both the population of atomic oxygen states at the $H_2 + O_2$ reaction and the reactivity of oxygen atoms towards H_2 for the formation of H_2O. The nature of the defects has not been directly investigated, but chemically the defect sites behave similar to kinks or steps on the Pt(1 0 0) single crystal surface. These results are expected to provide a better insight into the mechanism of rate oscillations in the $H_2 + O_2$ reaction on the Pt(1 0 0) nanoplane surfaces. FEM/FIM results have strongly suggested that the H_{ads}-induced (hex) $\rightarrow (1 \times 1)$ phase transition observed on the Pt(1 0 0) single crystal is the driving force for the isothermal oscillations found on that *nano*plane (1 0 0) surface.

5. Hydrogen spillover in H_2 oxidation on Pd–Ti^{3+}/TiO_2

5.1. The effect of oxygen vacancies Ti^{3+}-$\square_O/TiO_2$ on O_2 adsorption

In this section, the role of defects (Ti^{3+}-sites) in the active centers formation, their stabilization by the palladium nanoparticles and then defects participation in the $H_2 + O_2$ reaction have been studied on the TiO_x surface. The O_2 adsorption and the reaction of $O^{\delta-}_{2ads}$ molecular state as well as an O_{ads} atomic state with H_2 have been studied on the Ti^{3+}-$\square_O/TiO_2$ and Pd–Ti^{3+}-$\square_O/TiO_2$ surfaces. The effect of spillover phenomena ($H_{ads}/Pd \rightarrow O^{\delta-}_{2ads}/Ti^{3+}/TiO_2$) on the overall steady-state rate of H_2 oxidation has been studied as well. The results obtained in H_2 oxidation over the Pd(1 1 0) and Pd wire surfaces have been compared.

According to the XPS data, the reduction in the thin oxide layer (TiO_2/Ti, ~300 Å) following the heating in vacuum at 700 K leads to appearance of the state Ti $2p_{3/2}$ (Ti^{3+}-sites) with the binding energy E_B = 457.5 eV and formation of the oxygen-vacancy defect sites (Fig. 12a). The reduction of this oxide layer occurs due to the titanium atoms diffusion on the surface and oxygen one into the metal. The surface layer containing the Ti^{3+}-$\square_O$ defects is detected by UV photoemission as the state 0.8 eV below the Fermi level in the forbidden region (Fig. 12b-curve 2). The oxygen-vacancy defect sites are the active centers in O_2 dissociative adsorption and can be eliminated by oxygen adsorption at 300 K (Fig. 12b-curve 3).

Therefore, a low temperature study of O_2 adsorption and subsequent reactions at defect sites is necessary for detailed understanding of the catalytic properties of TiO_x surfaces. Two molecular γ- and α-states of the adsorbed oxygen (100 K) with $T_{des} \sim 140$ and ~240 K were found on such surface by TDS

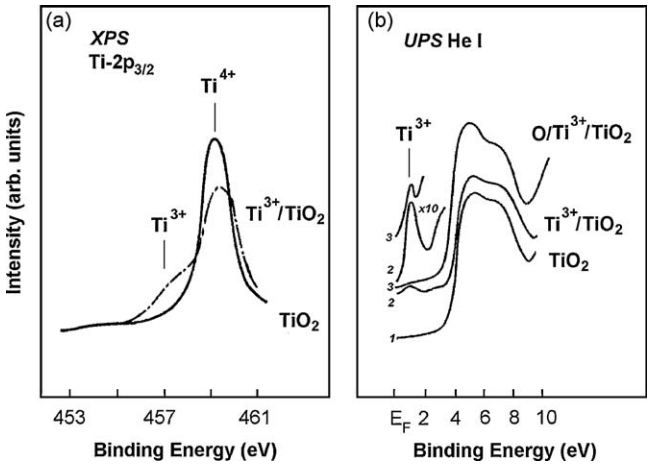

Fig. 12. (a) Ti $2p_{1/2}$ XPS spectra of the TiO_2/Ti thin layer taken after annealing in UHV at $T \sim 700$ K. (b) Changes in UV spectra caused by reduction of the TiO_2 thin layer (1) at 700 K (2) and oxygen adsorption on the Ti^{3+}/TiO_2 surface at 300 K (3), exposure 10^3 L [43].

(Fig. 13a). The molecular character of γ- and α-states was determined by means of isotopes. At the UV irradiation of the surface with light energy $2.8 < h\nu < 3.4$ eV the sharp photodesorption of O_2-peak was found to occur only from α-species as a result of reaction between holes (p^+) and α-$O^{\delta-}_{2ads}$. The concentration of the photosensitive oxygen state was about 10^{-2} ML. Fig. 13b presents the photodesorption spectra for the O_{2ads} layer at different stages of the thermal annealing from 100 to 300 K. The initial photodesorption of O_2-peak dramatically decreases as a result of thermal desorption and dissociation of α-$O^{\delta-}_{2ads}$ state with a simultaneous oxidation of the Ti^{3+}-sites at $T < 300$ K. The threshold energy for the O_2 photodesorption was at $h\nu \sim 3.0$ eV, corresponding to the band-gap of the bulk rutile TiO_2 (Fig. 13c).

5.2. The effect of Pd particles on the Ti^{3+}-$\square_O/TiO_2$ surface

Strong interaction of supported palladium particles with electron donor defects (Ti^{3+}-$\square_O$) over the oxide layer has been found to lead to the stabilization of these defects with respect to oxidation by oxygen [95]. According to the XPS data, from the

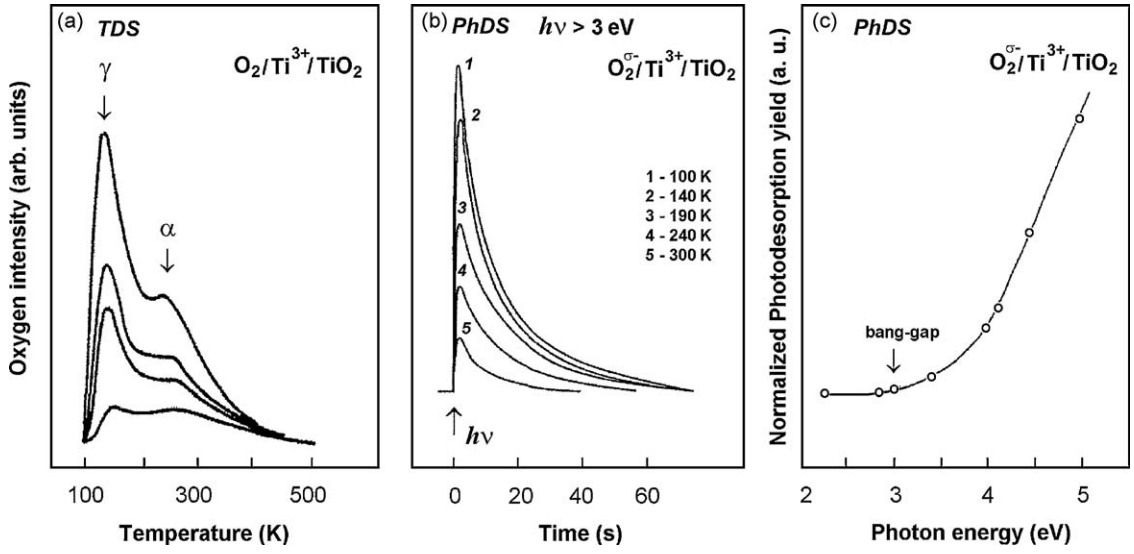

Fig. 13. (a) TD-spectra obtained after O_2 adsorption at 100 K. (b) Oxygen photodesorption yield from Ti^{3+}/TiO_2 (18 L, 100 K) as a function of annealing temperatures (T_a). Annealing time at T_a corresponds to 120 s. (c) The photon energy dependence of the oxygen photodesorption rate from Ti^{3+}/TiO_2 (18 L, 100 K). The photodesorption yield has been normalized to the photon flux at each photon energy value [43].

initial coverages θ_{Pd} = 0.06/0.3 ML there is an increase of the Pd $3d_{5/2}$ and Pd $3d_{3/2}$ lines intensity with their simultaneous shift by 0.5 eV to the smaller binding energy E_b (Fig. 14a, curves 1–4). After 700 K annealing (curve 5), the state of palladium on the Ti^{3+}-□O/TiO_2 surface is E_b (Pd $3d_{5/2}$) = 334.6 eV and in the neighborhood as for the bulk metal. The Ti^{3+} spectral regions are presented in Fig. 14a (XPS Ti-$2p_{3/2}$) and Fig. 14b (UPS He I). The Pd deposition is accompanied by diminution of the Ti^{3+} sites intensity (XPS: $I(Ti^{3+})/I(Ti^{4+})$) as a result of electron density transfer from the Ti^{3+}-□O electron donor defects to metal [96]. According to the UPS spectra with $E_b \sim 2.6$ eV, the state of palladium at $\theta \sim 0.1$ ML is characteristic of electron emission from d^9-state of single metal atoms supported on the oxide surface [97]. The analysis of difference UPS spectra shows the change of line width at half peak intensity from 1.6 eV (0.1 ML) up to 2.5 eV (0.3 ML) that is caused by increasing of the Pd particles size. Heat-up to 700 K is accompanied by electron photoemission near the Fermi level (curve 4), indicating the particles formation (<20 Å) with properties close to the bulk metal [36].

5.3. H_2 oxidation on palladium

Fig. 15a shows series of O_2 TDS spectra from Pd(1 1 0) single crystal surface. The several oxygen peaks are detected after different oxygen exposures at 100 K. Above a 0.3 L exposure of O_2, there are three peaks in the spectrum, around 125 (α-O_2 molecular state), 740 (β_1-O atomic state), and 815 (β_2-O atomic state) K. The β_2-peak at 815 K is seen due to recombination of O_{ads} surface atoms. The β_1-oxygen state has been attributed to subsurface oxygen ($O_{ads} + {}^*_v \rightarrow {}^*O_{sub}$), as indirectly indicated by work function measurements [98] and XPS [99]. Thermal desorption spectra of H_2 from Pd(1 1 0) surface obtained after exposure to hydrogen (2 L) at 100 K is shown in Fig. 15b. There are two desorption states: the α-state (225 K) and the β-state (320 K) resulted from recombination of chemisorbed atomic hydrogen [100]. The H_2O TPR spectra obtained in the reaction $H_{ads} + O_{ads}$ on Pd(1 1 0) are shown in Fig. 16a. Interaction of the O/Pd(1 1 0) atomic oxygen layer (0.2 L) with hydrogen (2 L) was determined to be accompanied by low temperature formation of H_2O with a desorption peak at $T \sim 250$ and hydrogen desorption at ~355 K.

For the purpose to compare the catalytic activities of palladium nanoparticles (Pd/Ti^{3+}/TiO_2) with a polycrystalline palladium surface (Pd wire) in the low temperature H_2 oxidation we have determined the rate of steady-state reaction at 2×10^{-7} mbar with ratio H_2:O_2 = 2:1 (Fig. 16b). The catalytic activity of Pd wire was studied in a separate all-glass ultrahigh vacuum chamber (1.5 L volume) with a residual pressure $< 10^{-10}$ mbar. It can be seen that

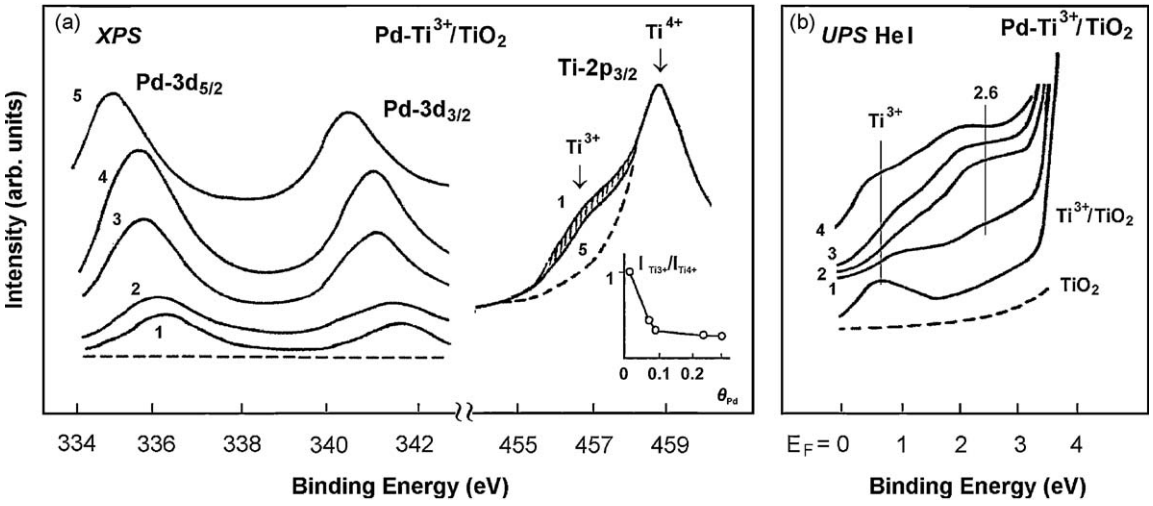

Fig. 14. (a) Pd $3d_{5/2}$ and Ti $2p_{1/2}$ XPS spectra of the Pd/Ti_i^{3+}/TiO_2 system as a function of Pd thickness (θ_{Pd} (curves 1–4): 0.06, 0.08, 0.24, 0.3 ML), recorded at 300 K. The upper curve (5) shows Pd $3d_{5/2}$ spectra after annealing for 120 s at T = 700 K. (b) UP valence band spectra of Ti^{3+}/TiO_2 surfaces after stepwise evaporation of Pd at 300 K with increasing of Pd coverages (θ_{Pd} (curves 1–3): 0.08, 0.24, 0.3 ML. The latter is determined from corresponding XPS intensities. The upper curve (4) shows the valence band spectra after annealing for 120 s at T = 700 K [43].

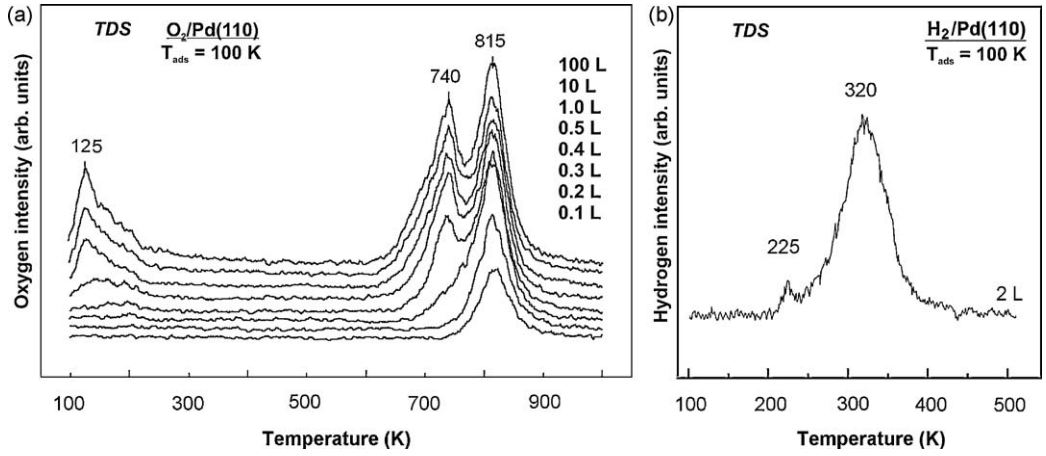

Fig. 15. (a) O_2 TD-spectra from Pd(1 1 0) dosed with different exposures of O_2 at 100 K. (b) TD-spectrum of hydrogen from a Pd(1 1 0) surface obtained after adsorption (2 L) at 100 K [47].

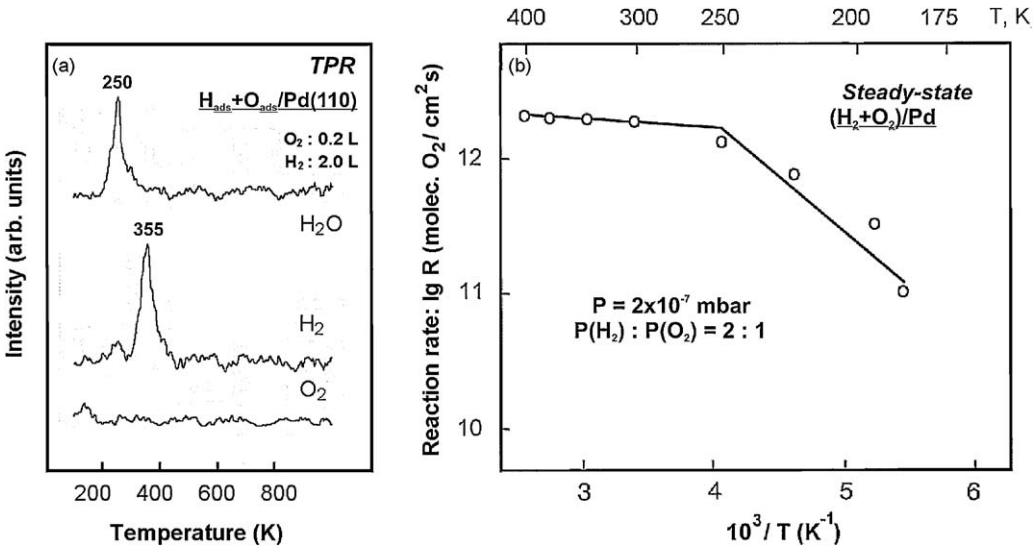

Fig. 16. (a) Series of TPR spectra of the H_2O molecules formation during H_{ads} + O_{ads} reaction on the Pd(1 1 0) surface obtained after low temperature O_2 and H_2 adsorption at 100 K. (b) Temperature dependence of the steady-state rate lg R (molec. O_2/cm^2 s) of hydrogen oxidation on Pd wire at $P = 2 \times 10^{-7}$ mbar ($P(H_2)$:$P(O_2)$ = 2:1).

over the temperature range 175–400 K the curve of lg R (R, reaction rate) versus temperature has a sharp break at $T \sim 250$ K, which indicates the transition from the oxygen (250–400 K) to hydrogen (175–250 K) side of reaction. The apparent activation energy (E_a) in the temperature interval 175–250 K is ca. 15 kJ/mol [3]. The obtained data indicate that the steady-state reaction occurs in the two regions depending on the ratio of reagent pressures. In the oxygen side, where $P(O_2) > P(H_2)$, the reaction rate is $R \sim P^2(H_2)/P(O_2)$, and the surface is predominantly covered with oxygen, whereas for the hydrogen side, where $P(O_2) < P(H_2)$, the reaction rate is $R \sim P(O_2)$, it is mainly covered with hydrogen [3]. It is believed that *spillover effect* of hydrogen from Pd nanoparticles into the supporting oxide surfaces (Ti^{3+}/TiO_2) is possible only in the range of $P(H_2) > P(O_2)$ for the H_{ads}-side of H_2 oxidation.

5.4. The hydrogen spillover effect on H_2 oxidation over Pd–Ti^{3+}/TiO_2

One might expect that in the Pd–Ti^{3+}/TiO_2 system owing to electron transfer ($Ti^{3+} \rightarrow$ Pd) the conversion of Ti^{3+} electron donor defects to oxidized Ti^{4+} ions should be accompanied by the losses of the TiO_x surface to adsorption ability in $O^{\delta-}_{2ads}$ state. However, the data presented in Fig. 17 (curve 1) show that the sharp photodesorption of O_2-peak ($\theta \sim 10^{-2}$ ML) proceeds from $O^{\delta-}_{2ads}$ oxygen adlayer (150 K) by the UV irradiation. Apparently there is a possibility of a reversible electron transition Pd $\rightarrow Ti^{3+} \rightarrow O^{\delta-}_{2ads}$ with the $O^{\delta-}_{2ads}$ state formation. The similar reversible electron transition is typical of the metal-complex compounds at replacement of the electron-donor ligands by electron-acceptor ligands [101]. The $O^{\delta-}_{2ads}$ state on the Pd–Ti^{3+}/TiO_2 surface is much more stable and exists up to temperatures of ca. 350 K (Fig. 17b). The increase of Ti^{3+}/TiO_2 defect stability to the oxidation by $O^{\delta-}_{2ads}$ is caused by electron-acceptor properties of Pd particles diminishing the electron density on the Ti^{3+}-$\square_O$ defects due to SMSI effect [35]. Since in Pd presence the transfer of the second electron on $O^{\delta-}_{2ads}$ is sharply impeded, then the defect oxidation in direction $O_2 \xrightarrow{e^-} O_2^- \xrightarrow{e^-} O_2^{2-} \rightarrow 2O^- \xrightarrow{e^-} 2O_{lattice}^{2-}$ accompanied by non-reversible disappearance of oxygen vacancies -$\square_O$ is unlikely.

Fig. 17a shows a set of curves for the isothermal reaction of H_2 with pre-adsorbed oxygen at 150 K over the Pd–Ti^{3+}/TiO_2 surface. The $O^{\delta-}_{2ads}$-state photodesorption intensity is used as a *test* for

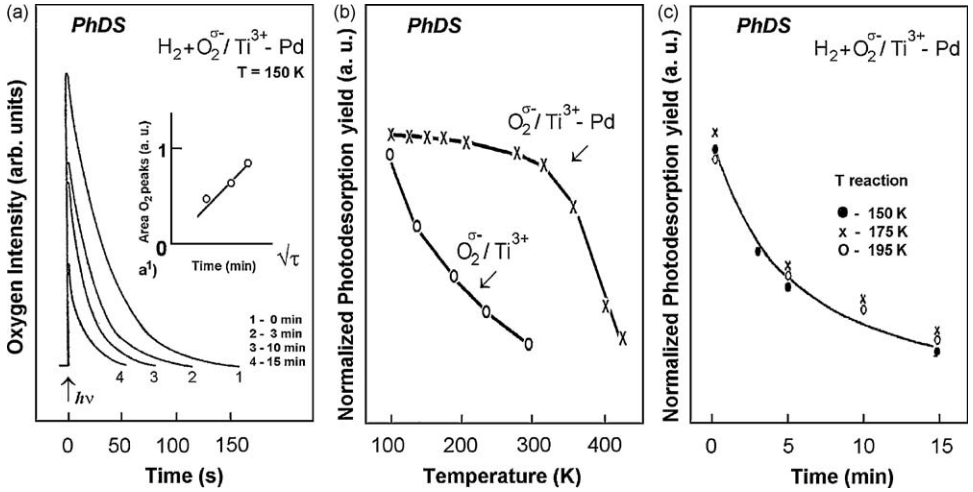

Fig. 17. (a) Oxygen photodesorption yields from Pd/Ti^{3+}/TiO_2 as a function of H_2+$O^{\delta-}_{2ads}$ reaction at 150 K and $P(H_2) = 1.3 \times 10^{-7}$ mbar. (1) Initial spectrum after O_2 adsorption at 100 K, 20 L. (2–4). Reaction time: (2) 3 min; (3) 10 min; (4) 15 min. (a^1) Rectification of difference square of curves 1–4. (b) Normalized oxygen photodesorption yield from the $O^{\delta-}_{2ads}/Ti^{3+}/TiO_2$ and $O^{\delta-}_{2ads}/Ti^{3+} - Pd/TiO_2$ surfaces (18 L, 100 K) as a function of annealing temperatures in UHV. Annealing time at T_a corresponds to 180 s. (c) Normalized oxygen photodesorption yields from $O^{\delta-}_{2ads}/Ti^{3+} - Pd/TiO_2$ surfaces (20 L) [43].

spillover studies. The reacting molecules are detected by the difference of the photo-peak areas for initial concentration (curve 1) and after reaction (curves 2–4). The reaction proceeds only in the palladium (θ_{Pd} = 0.3 ML) presence with the constant diminution of photo-peak intensity in time. Rectification in coordinates: the concentration of the reacted oxygen ($O^{\delta-}_{2ads}$ peak area) as a function of time ($\sqrt{\tau}$) indicates the diffusion availability associated with the hydrogen migration from Pd into the TiO_x surface (Fig. 17a[1]).

The hydrogen atoms transfer from metal to the support is considered to be the limiting stage in spillover phenomena [35]. H_2O molecules formation in the H_2 oxidation over support can proceed through the intermediates such as HO_2* radical [102]. The interaction of α-$O^{\delta-}_{2ads}$ molecular layer with hydrogen on the Pd/Ti^{3+}/TiO_2 surfaces in the temperature interval of 150–195 K is characterized by apparent activation energy close to zero (Fig. 17c). This reaction seems to involve the "protonate" hydrogen atoms (H^+/TiO_x) as a result of the spillover effect: H_{ads} atoms diffusion from Pd particles onto the TiO_x surface [35]. The α-$O^{\delta-}_{2ads}$ molecular state on the clean TiO_x surface appears to be non-reactive to hydrogen due to the absence of active centers (Pd) required for the H_2 dissociative adsorption.

It has been found that the low temperature H_2 oxidation on palladium ($T < 250$ K) results from the high reactivity of H_{ads} and O_{ads} atomic species (Fig. 16b). Under the steady-state reaction conditions at $P(H_2):P(O_2)$ = 2:1 in the temperature interval 175–250 K the Pd surface is covered by hydrogen (H_{ads}-side). Therefore, the overall rate of H_2 oxidation on the Pd/TiO_x system includes the rate on Pd particles and the contribution of spillover phenomena ($H_{ads}/Pd \rightarrow O_{2ads}/Ti^{3+}/TiO_2$).

The specific catalytic activity of Pd–Ti^{3+}/TiO_2 system at UV irradiation ($+h\nu(-\alpha - O^{\delta-}_{2ads}$ state)) is equal to 9.2×10^{11} molecules H_2O/cm^2 s at the following reaction conditions: T = 220 K, $P = 2 \times 10^{-7}$ mbar ($H_2:O_2$ = 2:1). In the dark ($-h\nu(+\alpha - O^{\delta-}_{2ads}$ state)) the reaction rate increases up to 1.0×10^{12} molecules H_2O/cm^2 s and approaches the specific catalytic activity of polycrystalline Pd wire [3]. A series of activity sets: $Ti^{3+}/TiO_2 << Pd \sim Pd/Ti^{3+}/TiO_2$ have been determined.

A probable mechanism of the $H_2 + O_2$/Pd–Ti^{3+}/TiO_2 reaction with participation of spillover effect.

H_2 oxidation on Pd nanoparticles	Spillover effect in H_2 oxidation on Ti^{3+}/TiO_2
1. $O_{2\ gas} + 2^* \rightarrow 2O_{ads}$	6. $H_{ads}(Pd) \xrightarrow{spillover} H_{ads}(TiO_2) + (Pd)$
2. $H_{2gas} + 2^* \rightarrow 2H_{ads}$	7. $H_{ads}(TiO_2) \xrightarrow{protonation} H^+(TiO_2) + e^-(Pd)$
3. $H_{ads} + O_{ads} \rightarrow OH_{ads} + ^*$	8. $O_{2gas} + (Ti^{3+}) \rightarrow O^{\delta-}_{2ads}(Ti^{3+})$
4. $H_{ads} + OH_{ads} \rightarrow H_2O_{ads} + ^*$	9. $2H^+(TiO_2) + O^{\delta-}_{2ads}(Ti^{3+}) \rightarrow [H_2O_2]^*_{ads} \rightarrow$
5. $H_2O_{ads} \rightarrow H_2O_{gas} + ^*$	$\rightarrow OH_{ads}(TiO_2) + OH_{ads}(Ti^{3+})$
	10. $H^+(TiO_2) + OH_{ads}(TiO_2) \rightarrow H_2O_{gas} + 2(TiO_2)$
	11. $H^+(TiO_2) + OH_{ads}(Ti^{3+}) \rightarrow H_2O_{gas} + (Ti^{3+}) + (TiO_2)$

5.5. Summary

Partially reduced titanium supports are particularly interesting in oxidation catalysis, because their surfaces reveal the increased oxidation activity due to an oxygen species associated with titanium oxide directly involved in the oxidation. It was shown that the deposition of Pd nanoparticles with the size <20 Å on the TiO_x surface leads to: (i) stabilization of surface defects Ti^{3+} (SMSI) with respect to oxidation; (ii) increase of thermal stability of the α-$O^{\delta-}_{2ads}$ state up to $T \sim 350$ K. One of the important functions of Pd nanoparticles in H_2 oxidation is the dissociation of hydrogen and oxygen molecules with the subsequent supply of the H_{ads} atoms into $O_{2ads}/Ti^{3+}/TiO_2$ system through spillover phenomena. The combination of metallic (Pd) and ionic sites (Ti^{3+}) provides the catalyst with molecular oxygen storage capacity. Two different parallel reaction routes through the atomic and molecular oxygen states in H_2 oxidation were found to proceed.

6. Summary and outlook

The reaction of hydrogen with oxygen on the Pt and Pd surfaces is surprisingly complex. We have explored different metal surfaces (single crystals, tips, nanoparticles) and have observed varied reaction regimes: steady-state, oscillatory, waves, spillover. Water formation as a result of the interaction between H_{ads} and O_{ads} atoms involves an OH intermediate. The reaction proceeds via L–H detailed mechanism in which adsorbed hydrogen atoms in the initial stage react with chemisorbed oxygen to form hydroxyls, which react with a second hydrogen atom to produce water. The DFT calculations demonstrate that the threefold hollow sites (fcc) for adsorption of H_{ads} and O_{ads} atoms are preferred on Pt(1 1 1). It is shown that OH-groups can occupy bridge site in Pt_2-$(OH)_{ads}$ bent structure compared to weakly bond energy site for H_2O_{ads} in Pt_1-(OH_2) on-top structure. The comprehensive study of H_2, O_2 adsorption and $H_2 + O_2$ reaction in a row: single crystals → tips → nanoparticles has shown the same nature of active centers over these metal surfaces. $H_2 + O_2$ reaction on the Pd–Ti^{3+}/TiO_2 model catalysts is a *spillover sensitive*. Through the hydrogen spillover from Pd nanoparticles to the Ti^{3+}/TiO_2 surface two different parallel reaction routes in $H_2 + O_2$ reaction can occur: on Pd particles and on the Ti^{3+}/TiO_2 support.

The great interest in self-oscillatory phenomena in oxidation reactions over metal surfaces is for a large part caused by the possibility to perform the catalytic processes more efficiently using unsteady-state operation. In the oscillating regime, the reaction mixture periodically affects the properties of metal surfaces. The oscillation cycles of the different products may have different states and surface phases with respect to each other, this can produce unvalued information on the mechanism of such reactions. Mechanisms of oscillatory oxidation reactions are connected (i) with a periodic change in surface structure (Pt(1 0 0): hex ⇔ 1 × 1), (ii) with subsurface oxygen formation (Pd(1 1 0): $O_{ads} \Leftrightarrow O_{sub}$) and (iii) associated with the "explosive" nature of interactions between adsorbed species. A common feature in all these mechanisms is the spontaneous periodical transitions of the metal from an inactive to a highly active state. Our experimental results show that the field electron and field ion microscope can serve as an *in situ* catalytic flow reactor in the 10^{-7} to 10^{-3} mbar total pressure regime.

FEM/FIM microscopy has been used to investigate the dynamics (self-oscillation, waves) of the surface phenomena associated with H_2 oxidation on a nanoscale level. The experimental results on Pt-tip surface demonstrate that the maximum rate of H_2O formation is attained in a traveling narrow zone between O_{ads} and H_{ads} layers. In this reaction zone the highest concentration of free Pt-centers is reached, which contribute to dissociative adsorption of H_2, O_2 and a rapid reaction with closely arranged H_{ads}, O_{ads} atoms. Our FEM results indicated a key role of stepped surfaces in initiation of such oscillations. The obtained results reveal the detailed mechanism of self-organization in $H_2 + O_2$ reaction on catalytically active Pt surfaces of hundred Angstroms size; the propagation of reaction-diffusion waves includes the participation of the different crystal nanoplanes and indicates an effective coupling of adjacent planes. It becomes possible to study catalysis on a nanoscale level, which is

necessary for the understanding of the mechanism of action of the highly dispersed supported metal catalysts having metal nanocrystallites 100–300 Å in size as active parts of the catalyst. This result will open new fields for the development of theoretical concepts of heterogeneous catalysis. The most exciting result of this work lies in the following: the appearance of regular waves is an amazing example of self-organization of a catalytic reaction on a metal particle with a size of some hundreds Å. For future studies, it is necessary to develop mathematical models based on the Monte Carlo techniques that makes to reflect easily the spatio-temporal dynamics of adsorbate distribution on different metal surfaces (single crystals, tips, nanoparticles), whose structure may transform under the action of the reaction medium.

Acknowledgements

This work is supported in part by RFBR Grant No. 08-03-00454, 08-03-00825, INTAS No. 05-109-5039 and Russian Science Support Foundation.

References

[1] G.K. Boreskov, J. Chim. Phys. 51 (1950) 759.
[2] P.R. Norton, in: D.A. King, D.P. Woodruff (Eds.), The Chemical Physics of Solid Surfaces and Heterogeneous Catalysis, vol. 4, Elsevier, Amsterdam, 1982, p. 27.
[3] V.V. Gorodetskii, V.A. Sobyanin, A.R. Cholach, M.Yu. Smirnov, Proc. VIII Intern. Congr. Catalysis vol. 3, Berlin (West), Verlag Chemie, (1984), p. 323.
[4] P.R. Norton, J. Catal. 36 (1975) 211.
[5] B.A. Morrow, P. Ramamurthy, J. Phys. Chem. 77 (1973) 3052.
[6] D.M. Collins, J.B. Lee, W.E. Spicer, J. Vac. Sci. Technol. 13 (1976) 266.
[7] T. Engel, H. Kuipers, Surf. Sci. 90 (1979) 181.
[8] E.M. Stuve, S.W. Jorgensen, R.J. Madix, Surf. Sci. 146 (1984) 179.
[9] G.E. Mitchell, J.M. White, Chem. Phys. Lett. 135 (1987) 84.
[10] B.A. Gurney, W. Ho, J. Chem. Phys. 87 (1987) 5562.
[11] T.A. Germer, W. Ho, Chem. Phys. Lett. 163 (1989) 449.
[12] V.V. Gorodetskii, M.Yu. Smirnov, A.R. Cholach, in: L. Guczi, F. Solymosi, P. Tetenyi (Eds.), New Frontiers in Catalysis, pt. B, Elsevier Science Publishers, 1993, p. 1587.
[13] C. Nyberg, C.G. Tengstål, J. Chem. Phys. 80 (1984) 3463.
[14] S. Völkening, K. Bedürftig, K. Jacobi, J. Wintterlin, G. Ertl, Phys. Rev. Lett. 83 (1999) 2672.
[15] J. Wintterlin, Adv. Catal. 45 (2000) 131.
[16] L.K. Verheij, M. Freitag, M.B. Hugenschmidt, I. Kempf, B. Poelsema, G. Gomsa, Surf. Sci. 272 (1992) 276.
[17] D.F. Padowitz, S.J. Sibener, Surf. Sci. 254 (1991) 125.
[18] G.B. Fisher, B.A. Sexton, Phys. Rev. Lett. 44 (1980) 683.
[19] B. Hellsing, B. Kasemo, V.P. Zhdanov, J. Catal. 132 (1991) 210.
[20] G. Ertl, Chem. Record 1 (2000) 33.
[21] V.P. Zhdanov, B. Kasemo, Surf. Sci. Rep. 20 (1994) 113.
[22] V. Gorodetskii, J. Lauterbach, H.-H. Rotermund, J.H. Block, G. Ertl, Nature 370 (1994) 276.
[23] A. Schaak, B. Nieuwenhuys, R. Imbihl, Surf. Sci. 441 (1999) 33.
[24] A. Schaak, R. Imbihl, J. Chem. Phys. 113 (2000) 9822.
[25] E. Schütz, F. Esch, S. Günther, A. Schaak, M. Marsi, M. Kiskinova, R. Imbihl, Catal. Lett. 63 (1999) 13.
[26] V.V. Gorodetskii, V.I. Savchenko, in: J.W. Hightower (Ed.), Proc. V Intern. Congr. on Catalysis, vol. I, North-Holland, Amsterdam, (1973), p. 527.
[27] V.V. Gorodetskii, V.A. Sobyanin, N.N. Bulgakov, Z. Knor, Surf. Sci. 82 (1979) 120.
[28] V.V. Gorodetskii, B.E. Nieuwenhuys, W.M.H. Sachtler, G.K. Boreskov, Appl. Surf. Sci. 7 (1981) 355.
[29] J.H. Block, W. Drachsel, N. Ernst, B. Sieben, V. Gorodetskii, Ber. Bunsenges. Phys. Chem. 99 (1995) 1363.
[30] J.H. Block, V.V. Gorodetskii, W. Drachsel, Recl. Trav. Chim. Pays-Bas. 113 (1994) 444.
[31] T. Vizart de Bocarmé, T. Bär, N. Kruse, Surf. Sci. 454–456 (2000) 320.
[32] T. Vizart de Bocarmé, T.-D. Chau, N. Kruse, Top. Catal. 39 (2006) 111.
[33] Y. Suchorski, W. Drachsel, Top. Catal. 46 (2007) 201.
[34] V.V. Gorodetskii, V.I. Elokhin, J.W. Bakker, B.E. Nieuwenhuys, Catal. Today 105 (2005) 183.
[35] S.J. Tauster, S.C. Fung, R.L. Garten, J. Am. Chem. Soc. 100 (1978) 170.
[36] C.R. Henry, Surf. Sci. Reports 31 (1998) 231.
[37] D.I. Kochubey, S.N. Pavlova, B.N. Novgorodov, G.N. Kryukova, V.A. Sadykov, J. Catal. 161 (1996) 500.
[38] W. Curtis Conner Jr., G.M. Pajonk, S.J. Teichner, Adv. Catal. 34 (1986) 1.
[39] S.C. Fung, J. Catal. 76 (1982) 225.
[40] T. Suzuki, R. Souda, Surf. Sci. 448 (2000) 33.
[41] M.Yu. Smirnov, V.V. Gorodetskii, Poverhnost 7 (1986) 21 (in Russian).
[42] G. Lu, A. Linsebigier, J.T. Yates Jr., J. Chem. Phys. 102 (1995) 4657.
[43] V.V. Gorodetskii, A.V. Matveev, Stud. Surf. Sci. Catal. 138 (2001) 85.
[44] V.P. Zhdanov, Surf. Sci. 500 (2002) 966.
[45] V.V. Gorodetskii, A.V. Matveev, P.D. Cobden, B.E. Nieuwenhuys, J. Mol. Catal. A: Chem. 158 (2000) 155.
[46] M.Yu. Smirnov, D. Zemlyanov, V.V. Gorodetskii, E.I. Vovk, Surf. Sci. 414 (1998) 409.
[47] V.V. Gorodetskii, A.V. Matveev, E.A. Podgornov, F. Zaera, Topics Catal. 32 (2005) 17.
[48] V. Gorodetskii, J.H. Block, W. Drachsel, M. Ehsasi, Appl. Surf. Sci. 67 (1993) 198.
[49] P.D. Cobden, V.V. Gorodetskii, B.E. Nieuwenhuys, Surf. Sci. 432 (1999) 61.
[50] Yu. Suchorski, R. Imbihl, V.K. Medvedev, Surf. Sci. 401 (1998) 392.
[51] P.D. Cobden, B.E. Nieuwenhuys, V.V. Gorodetskii, Appl. Catal. A: Gen. 188 (1999) 69.
[52] V.V. Gorodetskii, W. Drachsel, Appl. Catal. A: Gen. 188 (1999) 267.
[53] E.W. Müller, T.T. Tsong, Field Ion Microscopy, Elsevier, New York, 1969.
[54] W. Drachsel, C. Wesseling, V. Gorodetskii, J. Phys. IV 6 (1996) 31.
[55] N. Ernst, G. Bozdech, V. Gorodetskii, J.H. Block, Mass Spectr. Ion Process. 152 (1996) 185.
[56] V.V. Gorodetskii, G.I. Panov, V.A. Sobyanin, N.N. Bulgakov, React. Kinet. Catal. Lett. 9 (1978) 239.
[57] H. Steininger, S. Lehwald, H. Ibach, Surf. Sci. 123 (1982) 1.
[58] J. Schmidt, Ch. Stuhlmann, H. Ibach, Surf. Sci. 284 (1993) 121.
[59] Ch. Romainczyk, J.R. Manson, K. Kern, K. Kuhnke, R. David, P. Zeppenfeld, G. Gomsa, Surf. Sci. 336 (1995) 362.
[60] J.L. Gland, M.R. McClellan, F.R. McFeely, J. Chem. Phys. 79 (1983) 6349.
[61] H.P. Bonzel, G. Brodén, G. Pirug, J. Catal. 53 (1978) 96.
[62] D.Yu. Zemlyanov, M.Yu. Smirnov, V.V. Gorodetskii, Catal. Lett. 43 (1997) 181.
[63] B. Pennemann, K. Oster, K. Wandelt, Surf. Sci. 249 (1991) 35.
[64] A.B. Anton, D.C. Cadogan, J. Vac. Sci. Technol. A 9 (1991) 1890.
[65] L.K. Verheij, M.B. Hugenschmidt, Surf. Sci. 324 (1995) 185.
[66] G. Gilarowski, W. Erley, H. Ibach, Surf. Sci. 351 (1996) 156.
[67] K. Bedürftig, S. Völkening, Y. Wang, J. Wintterlin, K. Jacobi, G. Ertl, J. Chem. Phys. 111 (1999) 11147.
[68] M.Yu. Smirnov, V.V. Gorodetskii, A.R. Cholach, D.Yu. Zemlyanov, Surf. Sci. 311 (1994) 308.
[69] J.L. Gland, B.A. Sexton, G.B. Fisher, Surf. Sci. 95 (1980) 587.
[70] T. Zambelli, J.V. Barth, J. Wintterlin, G. Ertl, Nature 390 (1997) 495.
[71] M. Hock, V. Seip, I. Bassignana, K. Wagemann, J. Küppers, Surf. Sci. 177 (1986) L978.
[72] A.F. Carley, P.R. Davies, M.W. Roberts, K.K. Thomas, Surf. Sci. 238 (1990) L467.
[73] A.A. Gokhale, S. Kandoi, J.P. Greeley, M. Mavrikakis, J.A. Dumesic, Chem. Eng. Sci. 59 (2004) 4679.
[74] A.A. Sametova, V.M. Tapilin, V.V. Gorodetskii, S.E. Malyhin, III Intern. Conf. Catalysis: Fundamentals and application, Novosibirsk, Russia, July 3–8, (2007), p. 96, Abstracts OP-1-19.
[75] G.S. Karlberg, F.E. Olsson, M. Persson, G. Wahnström, J. Chem. Phys. 119 (2003) 4865.
[76] D.C. Ford, Y. Hu, M. Mavrikakis, Surf. Sci. 587 (2005) 159.
[77] G. Ertl, P.R. Norton, J. Rüstig, Phys. Rev. Lett. 42 (1982) 177.
[78] P.R. Norton, J.A. Davies, D.K. Creber, C.W. Sitter, T.E. Jackman, Surf. Sci. 108 (1981) 205.
[79] E. Ritter, R.J. Behm, G. Potschke, J. Wintterlin, Surf. Sci. 181 (1987) 403.
[80] W. Hösler, E. Ritter, R.J. Behm, Ber. Bunsenges. Phys. Chem. 90 (1986) 205.
[81] A. Borg, A.-M. Hilmen, E. Bergene, Surf. Sci. 306 (1994) 10.
[82] T.T. Tsong, Atom-Probe Field Ion Microscopy, Cambridge University Press, Cambridge, 1990.
[83] G.L. Kellogg, Surf. Sci. 177 (1986) L1021.
[84] K. Kuhnke, K. Kern, G. Comsa, Surf. Sci. 343 (1995) 44.
[85] P.N. Norton, J.A. Davies, D.P. Jackson, N. Matsunami, Surf. Sci. 85 (1979) 269.
[86] S.L. Bernasek, G.A. Somorjai, J. Chem. Phys. 62 (1975) 3149.
[87] K. Christmann, G. Ertl, Surf. Sci. 60 (1976) 365.
[88] V. Gorodetskii, J.H. Block, W. Drachsel, Appl. Surf. Sci. 76/77 (1994) 129.
[89] B. Sieben, G. Bozdech, N. Ernst, J.H. Block, Surf. Sci. 352–354 (1996) 167.
[90] H.J. Kreuzer, R.L.C. Wang, Z. Phyz. Chem. 202 (1997) 127.
[91] K. Heiz, E. Lang, K. Strauss, K. Müller, Appl. Surf. Sci. 11/12 (1982) 611.
[92] Y. Suchorski, W. Drachsel, V.V. Gorodetskii, V.K. Medvedev, H. Weiss, Surf. Sci. 600 (2006) 1579.
[93] V.P. Zhdanov, B. Kasemo, Surf. Sci. 496 (2002) 251.
[94] V.P. Zhdanov, Catal. Lett. 93 (2004) 135.
[95] M.Yu. Smirnov, K.I. Zamaraev, V.V. Gorodetskii, Poverkhnost 5 (1991) 41 (in Russian).
[96] J.A. Horsley, J. Am. Chem. Soc. 101 (1979) 2870.
[97] M.G. Mason, L.J. Gerenser, S.-T. Lee, Phys. Rev. Lett. 39 (1977) 288.
[98] J.-W. He, P.R. Norton, Surf. Sci. 204 (1988) 26.
[99] I.Z. Jones, R.A. Bennett, M. Bowker, Surf. Sci. 439 (1999) 235.
[100] J.-W. He, P.R. Norton, Surf. Sci. 195 (1988) L199.
[101] J.S. Valentino, Chem. Rev. 75 (1973) 235.
[102] H.D. Gesser, L. Krucznski, J. Phys. Chem. 88 (1984) 2751.